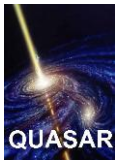

QUASAR Deliverable D4.3

Combined secondary interference models

Project Number:	INFSO-ICT-248303
Project Title:	Quantitative Assessment of Secondary Spectrum Access - QUASAR
Document Type:	

Document Number:	ICT-248303/QUASAR/WP4/D4.3/120331
Contractual Date of Delivery:	31.03.2012
Actual Date of Delivery:	31.03.2012
Editors:	Konstantinos Koufos (Aalto)
Participants:	Riku Jäntti (Aalto), Konstantinos Koufos (Aalto), Jonas Kronander (EAB), Evanny Obregon (KTH), Kalle Ruttik (Aalto), Yngve Selén (EAB), Ki Won Sung (KTH), Jens Zander (KTH)
Workpackage:	WP4
Estimated Person Months:	24 MM
Security:	PU[1]
Nature:	Report
Version:	1.0
Total Number of Pages:	69
File:	QUASAR_D4.3_120331

Abstract

The main requirement for secondary spectrum sharing is interference control. The interference control requires a good model for estimating the aggregate interference from all secondary transmitters. The aggregate interference to the primary receivers becomes the key bottleneck to secondary spectrum usage. The existing interference models for primary-secondary spectrum sharing are relatively complex and do not allow to study the impact of aggregate interference under massive use of secondary spectrum. In the present deliverable two novel interference models are proposed; the exclusion region model and the power density model The exclusion region model is applicable for low-powered devices such as WLAN type and femtocell secondary users. It enables the users to decide independently from each other whether to transmit or not. The exclusion region model is validated in the radar and the aeronautical

[1] Dissemination level codes: **PU** = Public
PP = Restricted to other programme participants (including the Commission Services)
RE = Restricted to a group specified by the consortium (including the Commission Services)
CO = Confidential, only for members of the consortium (including the Commission Services)

spectrum and found to predict well the generated interference at the primary receivers. The second model, the power density model allows reducing the implementation complexity in the database for secondary power allocation and interference control. The reason being, that the transmission of each secondary user is not considered individually. The secondary users are clustered together and the aggregate interference is described as an integral over the secondary deployment area. Both interference models will serve as input to WP5 for assessing the amount of available spectrum in various primary-secondary spectrum sharing scenarios. They may be used to study the impact of secondary transmissions under massive use of spectrum, which is ultimately the decisive factor for the commercial feasibility of any secondary service.

Keywords List

Aeronautical spectrum, aggregate interference modelling, distance measuring equipment, exclusion region model, Fenton-Wilkinson approximation method, moment matching techniques, Poisson point process, spatial power density model

Executive Summary

In deliverables D4.1 and D4.2 we proposed schemes for sharing the available spectrum opportunity between multiple competing or cooperating secondary systems. A spectrum sharing scheme would be used to provide commercial secondary services only if it is scalable. In order to assess its scalability, one has to study whether the generated interference in a scenario where a lot of transmitters are around and use the secondary spectrum can be tolerated at the primary receivers. This deliverable helps to do that by providing the models for computing the aggregate secondary interference at the primary receivers.

Firstly, a model of aggregate interference based on the cumulant approximation and including exclusion region for a single victim primary receiver is proposed. The exclusion region, or no-talk region, is defined as the area where the transmission of secondary users is not allowed. The model is applicable for low-power indoor secondary devices such as Wi-Fi and femtocell users that spread over a large area surrounding the primary victim. The model is validated by Monte Carlo simulations in the radar and the aeronautical bands. It can be used in a database-aided spectrum allocation scheme for estimating the distribution of aggregate interference and deciding whether particular secondary user can utilize the spectrum or not.

Secondly, a model for estimating the aggregate interference based on the spatial power density emitted from the secondary deployment area is proposed. The secondary users are considered to be deployed either in a cellular layout or in WLAN like layout. The model groups nearby located transmitters and describe the aggregate interference as a function of the spatial power density emitted from the secondary deployment area. In this way the precise location of secondary transmitters inside their deployment area is not needed and the computational complexity is reduced. The power density model for interference control is applicable in a database-based spectrum allocation scheme and can be used to reduce the implementation complexity in the database.

In Section 2 the state of the art in aggregate interference modelling is reviewed. The distribution of the aggregate interference under the exclusion region model is derived in Section 3.1 and under the spatial power density model in Section 3.1. In Section 4.1 the exclusion region model is modified to incorporate the impact of heterogeneous secondary user densities. The applications of the model in the radar spectrum (e.g. aircraft control and weather forecast radars) and in the aeronautical spectrum (e.g. DME for aeronautical navigation) are demonstrated in Section 4.2 and Section 4.3 respectively. It is shown that the exclusion region model approximates well the distribution of the aggregate interference.

In Section 5.1 the spatial power density model is validated by Monte Carlo simulations in the TV spectrum. It is shown that for relatively many secondary transmitters and simple power law based attenuation the spatial power density is sufficient to estimate the first two moments of the aggregate interference distribution. In Section 5.2 the power density model is used to allocate the transmission power level at the secondary transmitters. It is shown that the allocated transmission power levels do not generate harmful interference at the TV receivers. In Section 5.3 the terrain morphology is taken into consideration in the propagation path loss. It is illustrated that nearby located transmitters have highly correlated path loss values to the TV test points and can subsequently be clustered together. The power density emitted from each cluster of transmitters is sufficient to describe the interference generated at the TV receivers. In Section 5.4 the power density method is compared to the current ECC approach for secondary transmission power allocation. It is shown that the ECC approach may violate the TV protection criteria while the power density approach has built-in interference control. In addition, the power density approach can result in higher transmission power levels allocated to the secondary transmitters compared to the existing ECC method. In Section 5.5 a method to allocate the transmission power at the cellular secondary base

stations is proposed while taking into account the self-interference of the cellular system. It is shown that the transmission power levels outside of the TV protection area are about the same. In Section 5.6 the impact of non-uniform spatial service demand in the distribution of the aggregate interference is studied. It is shown that a clustered Poisson point process (PPP) process with relatively few clusters is able to capture the impact of non-uniform spatial service demand. Finally, Section 6 concludes the deliverable with a summary and discussion of the main results.

Contributors

First name	Last name	Company	Email
Jonas	Kronander	Ericsson AB	jonas.kronander@ericsson.com
Kalle	Ruttik	Aalto	Kalle.ruttik@aalto.fi
Konstantinos	Koufos	Aalto	Konstantinos.koufos@aalto.fi
Riku	Jäntti	Aalto	Riku.jantti@aalto.fi
Ki Won	Sung	KTH	sungkw@kth.se
Evanny	Obregon	KTH	ecog@kth.se
Yngve	Selén	Ericsson AB	yngve.selen@ericsson.com
Jens	Zander	KTH	jenz@kth.se

Table of contents

Acronyms

BS	Base station
CDF	Cumulative distribution function
CDMA	Code division multiple access
CEPT	European conference of postal and telecommunications administrations
CSMA	Carrier sense multiple access
DME	Distance measuring equipment
DTV	Digital TV
ECC	European communication committee
EIRP	Effective isotropic radiated power
FCC	Federal communication committee
FW	Fenton-Wilkinson
ITM	Irregular terrain model
MAC	Medium access control
PDF	Probability distribution function
PPP	Point Poisson process
RF	Radio frequency
RV	Random variable
SINR	Signal to interference and noise ratio
SIR	Signal to interference ratio
TVWS	TV white space
WLAN	Wireless local area network
WSD	White space device

1 Introduction

The aggregate interference to the primary receivers is the key bottleneck to secondary spectrum usage. A spectrum sharing scheme would be used to provide commercial secondary services only if it is scalable. In order to assess its scalability, one has to study whether the generated interference in a massive use of secondary spectrum can be tolerated at the primary receivers. This reveals the need for interference models in a primary-secondary system set up. In this deliverable the state of the art in interference modelling is reviewed and two new models for aggregate interference computation are proposed.

Firstly, the exclusion region model can be applied to estimate the aggregate interference in the scenario where multiple secondary transmitters interfere with a single primary receiver. A practical example is low-power secondary usage of radar and aeronautical spectrum. We propose a sharing scheme, sensing aided by geo-location databases, where each secondary transmitter decides whether to transmit or not based on a single interference threshold. Inside the exclusion region, the secondary users are not allowed to transmit. The shape and size of the exclusion region will highly depend on the spatial distribution of the secondary user and the level of knowledge or information about the propagation loss and the primary victim characteristics. The exclusion region model is modified to analyse the impact of different spatial distributions and different levels of knowledge on the aggregate interference.

Secondly, a model for estimating the aggregate interference based on the spatial power density emitted from the secondary deployment area is proposed. The idea is to group nearby located transmitters and describe the aggregate interference as a function of the spatial power density. The proposed method allows neglecting the precise location and transmission power level of each individual secondary transmitter. In this way, the amount of computations for estimating the aggregate interference is reduced.

In the absence of secondary transmissions the primary receivers may experience the primary system's self-interference. The difference between the self-interference level and the maximum interference level not violating the protection criteria of primary receivers is called the interference margin. The interference margin can be expressed as a function of the permitted spatial power density emitted from the secondary area. If the spatial distribution of secondary transmitters is available, the permitted power density can be mapped to the transmission power level for each individual secondary transmitter. In Section 3.1 it is shown how to allocate the transmission power level to cellular base stations and randomly located secondary transmitters.

The interference margin can be treated as an available resource. In the presence of multiple secondary areas the power density allocation to each area can be interpreted as a resource sharing problem.

The power density model along with the concept of interference margin makes the power allocation to secondary transmitters hierarchical. The database can allocate a fraction of the available interference margin to each secondary area based on the service demand, user density, etc. The allocated interference margin can be converted to the permitted power density value emitted from that area. The transmission power allocation to secondary transmitters inside that area can be delegated to some other local entity. The entity can allocate the power levels under the constraint that the total emitted power density does not exceed the permitted density. Only the power density or equivalently the allocated interference margin has to be communicated from the database to each entity. In this way the signalling communication overhead between the database and multiple local entities is reduced.

In Section 5.1 the spatial power density method is used to compute the aggregate interference from a cellular secondary system's downlink at the TV receivers. A simple channel model incorporating power law based attenuation and slow fading is utilized. It is assumed that the transmissions of all cellular base stations are described by the same

channel model. For validating the power density model we compute the moments of the aggregate interference by using integration over the secondary deployment area and direct summation given the locations of secondary base stations. We study the impact of the density of base stations on the approximation error for the first two moments of the aggregate interference. The impact of shadowing correlations to the approximation error is also demonstrated.

The power density method will be used to simplify the transmission power level allocation at the secondary devices while, at the same time, controlling the aggregate interference at the TV receivers. The allocated power density to an area can be mapped to the transmission power level of each transmitter inside that area if the spatial distribution of secondary transmitters is known. In Section 5.2 we allocate the transmission power level at cellular base stations by using the power density method. The aggregate interference is approximated to follow the log-normal distribution and its first two moments are written as a function of the spatial power density. The power density and subsequently the transmission power levels are computed such that the entire interference margin at the TV test points is utilized. The maximum permitted transmission power level is also computed by means of Monte Carlo simulations and the results are compared.

In reality, the propagation path loss is affected due to obstruction, scattering, terrain irregularities, etc and complex channel models should be used to account for these phenomena. In this kind of environment the power density may not be sufficient for describing the interference generated from a large area. In Section 5.3 the terrain morphology is taken into consideration in the propagation path loss. We utilize the Longley-Rice propagation model along with the ground elevation information data. We study how to split the secondary deployment area into multiple clusters such that the spatial power density emitted from a cluster is sufficient to describe the interference contributed from that particular cluster. Then, the aggregate interference can be computed as a sum of the interference contributed from each cluster.

The ECC has proposed a power allocation method for secondary transmitters operating in the TVWS. The current power allocation proposal by ECC does not include a particular algorithm for controlling the aggregate interference at the TV receivers. Only the limited cases of two to four simultaneous secondary transmissions are considered. For a higher number of simultaneous transmissions the ECC method proposes to control the aggregate interference by means of an additional safety margin. Because of that, the protection of the TV receivers is not sufficient in all cases. In Section 5.4 the proposed power density method is compared to the current ECC approach in terms of transmission power level allocation and TV receivers' protection.

The current rule by ECC adopts a location-based rule for setting the transmission power level to the secondary users. The further the secondary user is located from the TV coverage cell border, the higher transmission power it can utilize. The Federal Communication Committee (FCC) in US adopts a fixed power allocation rule with a protection distance around the TV coverage cell border. Both rules do not consider the self-interference in the secondary network while setting the transmission power level to the secondary users. In Section 5.5, unlike the existing ECC and FCC rules, we propose a method to allocate the transmission power at the secondary users while taking into account the self-interference of the secondary system. Our approach is illustrated in a cellular secondary system.

The operation of WLAN type of secondary users in the TVWS has been already recognized as a potential spectrum sharing scenario with clear business impact [1]. In order to assess the viability of this scenario we need to study the distribution of the aggregate interference at the TV receivers in a massive use of TV spectrum. To get a first assessment of aggregate interference, the complicated WLAN MAC is ignored. A Poisson point process (PPP) is used to model the distribution on of aggregate interference from randomly located and non-synchronous transmitters. However, a PPP

assumes that the transmitters are uniformly distributed inside their deployment area. Because of that, a PPP model is not sufficient to capture the statistics of the interference distribution in environments with non-uniform spatial service demand. One way to overcome this issue is to consider a clustered PPP process. The clustered PPP process describes the aggregate interference as a sum of the interference from multiple secondary clusters. Our study is illustrated in an environment incorporating terrain-based propagation channel model.

2 Review of interference modelling

Traditionally, interference models have been developed to describe the generated interference within a wireless data network. The secondary spectrum usage creates a need to model the interference between different types of systems. In order to be applicable in the primary-secondary system setup the, the single system interference models should be modified.

In Section 2.1 the general method to model the interference inside a wireless data network is presented. In Section 2.2 some of the models used to describe the generated interference from secondary to primary spectrum using systems are reviewed.

In a simple scenario, the locations of secondary transmitters are known and the only randomness in the generated interference comes from the channel fading. In that case, the distribution of the aggregate interference can be computed as a convolution of the individual interference distributions. In Section 2.3 the accuracy of the Fenton-Wilkinson (FW) method for approximating the distribution of the sum of log-normal random variables (RVs) is discussed. The reason being, that the FW method will be utilized both by the exclusion region and the power density model in Section 4 and Section 4.1 respectively.

2.1 Interference models from wireless networks

The aggregate interference I_{tot} at a victim receiver can be read as:

$$I_{tot} = \sum_{i=1}^{N} I_i = \sum_{i=1}^{N} \nu_i \cdot P_i \cdot g(r_i) \qquad (2\text{-}1)$$

where N is the total number of transmitters, ν_i is the activity of the i th interfering transmitter, $P_i, g(r_i)$ the transmission power level and the channel attenuation respectively. The channel attenuation is a function of the distance r_i between the i th interferer and the victim receiver.

The components for the computation of the aggregate interference are shortly explained below:

- ν_i : The interferers will not be active all the time. Their activity depends on the traffic intensity and the access protocol. The parameter ν_i is fractional between zero and one and describes the activity factor of a single transmitter.
- P_i : The transmission power level is determined based on the power control algorithm.
- $g(r_i)$: The attenuation in the radio channel usually consists of three terms: distance-based attenuation, small-scale and large-scale fading.

The nature of the above components (statistical or deterministic) would determine the nature of the generated interference. If the location, the activity, the transmission power and the attenuation in the channel are known for all the transmitters, the aggregate interference can be computed by using direct summation. For a large number of transmitters the direct summation can be time consuming. In addition, the exact propagation pathloss between transmitter and receiver is usually not available and probability distributions are used to model the impact of the fading. Due to these reasons, statistical-based interference modelling is utilized.

A statistical interference model describes one or more of the above factors by using probability distributions. In a simple case, the transmitters are always active, their locations are fixed and there is no power control. In that case, the only source of

randomness is due to the radio channel fading. The distribution of the aggregate interference can be computed as the convolution of the distributions describing the fading for each individual interferer. Unfortunately, such convolution does not always have a closed-form expression and approximations have been proposed.

The effects of large-scale fading are usually modelled by a log-normal random variable. The exact distribution of the sum of log-normal random variables is not known. The two most common methods for finding the approximation of the sum of log-normal random variables are the FW and the Schwartz-Yeh method. The FW method forces the first two moments of the aggregate interference distribution to be equal to the sum of the individual moments in the linear domain [26]. On the other hand, the Schwartz-Yeh method computes the approximation in the logarithmic domain [2]. A study of aggregate interference distribution with Gamma distributions for the fading can be found in [3] while for Rayleigh, Rician, log-normal and Nakagami fading can be found in [4].

If the locations of the transmitters are known, the computation of the aggregate interference through approximations turns out to be relatively simple. Because of that, other system properties can be also incorporated into the interference computation. For instance, the impact of power control and activity factor on the generated interference can be found in [5] and [8] respectively.

If the locations of the interfering transmitters are unknown, the distribution of the distances to the victim receivers affects the distribution of the aggregate interference. In that case, a stochastic model for the node locations (i.e., a spatial point process) is needed. Spatial point processes are the generalization of point processes indexed by time, to higher dimensions, such as 2-D space. If the interferers are located randomly in their deployment area and transmit independently from each other, then the interference can be computed from the PPP model. A PPP model is popular due to its analytical tractability but it is only suitable for describing the generated interference from ALOHA type of access schemes.

Most access schemes do not allow arbitrary transmissions. For instance, according to CSMA/CA, only one transmitter can get a chance to access the channel among multiple transmitters with overlapped carrier sensing regions. This kind of spatial filtering can be modelled by a Matern process [11]. Unlike the PPP, the Matern process is not analytically tractable. Also, in [12][13], the homogeneous PPP is modified to the so-called hardcore models [14] where a minimum node separation is properly applied. Poisson cluster process can be used when nodes are not distributed randomly but they tend to form clusters [10].

Instead of modelling the distribution of the aggregate interference one can model directly its effect. In [9] the distinction is made between the protocol and the physical models. The protocol model bypasses the complex interference computation process by enforcing protection areas around each receiver. The model determines the nature of the interference (harmful or not) only between pairs of communication links. If the interfering transmitter is outside the protection area of the victim receiver it does not generate harmful interference. Due to its simplicity, the protocol model can be used to study the performance of higher layer protocols. It is also suitable for the construction of the so-called interference graphs giving rise to graph-based interference models. As opposed to the protocol model, the physical model computes the SINR at each victim receiver and thus, it captures the impact of aggregate interference. The physical model allows studying more accurately the scheduling and the power control problems.

2.2 Modelling aggregate interference from secondary systems

The models developed to study the interference in wireless data networks have been modified to study the interference in a primary-secondary system set up. The basic difference is that the secondary transmitters are deployed outside the primary protection area.

In [15] the aggregate interference is computed for a cellular secondary system's downlink to the TV cell border. The authors investigate the impact of the density of the cells and the impact of the primary system's protection distance to the generated interference. Unlike [15] where the number of interferers is finite, the interference in [16] is computed from an infinite sea of secondary transmitters. The "sea" model allows computing the aggregate interference by integrating over the secondary deployment area. In general, such an integral is not analytically solvable. In [16] a closed-form solution, describing interference from a half-plane is derived. It is interesting to note that the interference from the "sea" can be described as the interference from a single transmitter with an increase in the pathloss attenuation exponent by a factor of two. The results of [16] are also validated in [17]. In [15][16][17] the transmission power levels of the secondary transmitters are assumed to be fixed, and the slow fading is ignored.

An alternative treatment of the aggregate interference modelling is based on the usage of the PPP model. Unlike traditional PPP models the secondary system transmitters are located outside of the primary system's protection area. The closed-form solution of the PPP-based interference model can be found in [18]. Therein, the moments of the interference distribution are found by integrating over a half plane. The PPP model indicates that for certain cases the interference distribution resembles a Gaussian distribution. The Gaussian approximation is suitable for a relatively high density of secondary transmitters [19]. In [7] the aggregate interference is approximated to follow a shifted log-normal distribution. The impact of a power control algorithm in the statistics of the aggregate interference for secondary transmitters deployed according to a PPP is investigated in [6].

2.3 Fenton-Wilkinson approximation

There exist numerous numerical approximations where the sum of log-normally distributed variables is approximated with another lognormal variable [25]. One of the first of these the Fenton-Wilkinson (FW) approximation [26] is derived by matching the first and second moments of the lognormal approximation with the sum of lognormal variables. The FW approximation is particularly interesting to use in the context of interference modelling for secondary usage of spectrum for several reasons. First, it is efficiently computed in closed-form. This is highly important, e.g., when computing the aggregate interference to a large set of points (e.g., when computing the probabilities of harmful aggregate interference for an area).

Second, perhaps even more importantly, the FW approximation is known to provide good approximations for the upper tails of the probability distribution [25]. This is highly relevant when modelling secondary interference to primary users since one typically then looks at a situation for which the probability of harmful interference must not exceed a low number (e.g., 0.5% or similar). For such a case it is of little importance if the approximation precision is lower towards the middle or lower parts of the probability distribution function. This behaviour is illustrated in Figure 2-1.

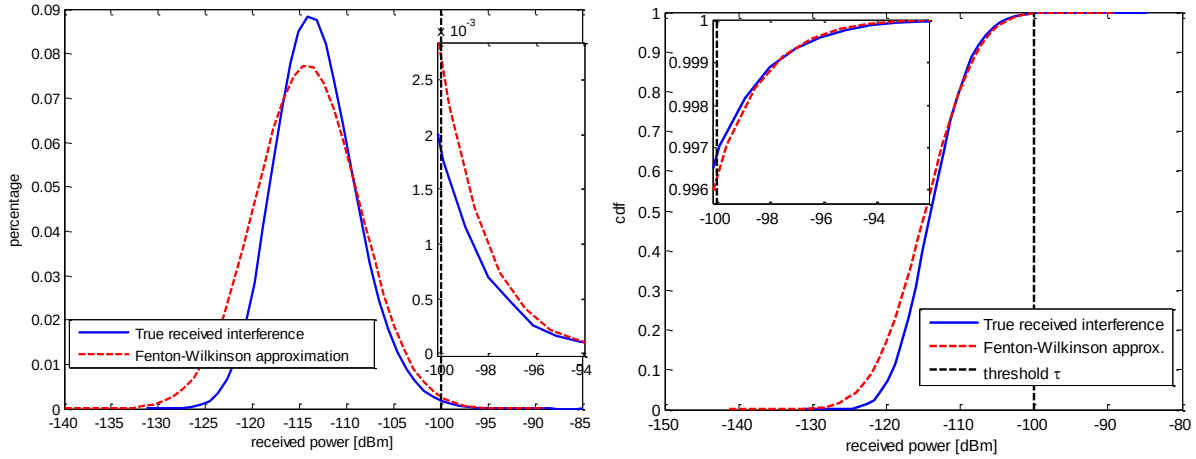

Figure 2-1: Comparison between the Fenton-Wilkinson approximation and Monte Carlo simulations of the distribution of aggregated interference generated from five secondary transmitters.

It is sometimes claimed that the FW approximation breaks down when the summed lognormal components have standard deviations greater than 4 dB. However, as discussed and shown in [27], this only concerns the FW approximation's ability to accurately estimate the first and second moments of the sum of lognormal variables and does not imply that the estimation of the CDF (cumulative density function) is poor under these conditions.

Figure 2-1 shows the probability distribution (left) and cumulative distribution (right) functions of the received power from 5 transmitters under lognormal fading with log-normally distributed channels having standard deviations of σ =7 dB. The red dashed curves show the FW approximation and the blue solid curves show the actual received power (as obtained by Monte Carlo simulation). The dashed black line illustrates an aggregated interference threshold, which is not to be exceeded with a probability greater than 0.5%. It can be seen that the FW approximation has high precision towards the upper (right) tail of the distribution. This also confirms the good behaviour of the approximation even for standard deviations above 4dB. The figures are results from studies further described in [21].

In [21] the FW approximation is studied within the context of an optimization procedure for computing upper power limits for individual white space transmitters when keeping the aggregate interference below a given threshold. The results from this study illustrate that the FW approximation is working well when working with the upper parts of the probability distribution.

The FW approximation has further been put to use in the numerical evaluations of the aggregated interference in the distributed power allocation in [22], as well as in the power adaptation strategy in [23].

For sake of completeness we shortly outline the FW approximation below following [24]. We start by writing the total aggregated interference in exponential form:

$$I_{tot} = \sum_{i=1}^{N} I_i = \sum_{i=1}^{N} e^{Y_i} \approx e^{Z} \qquad (2\text{-}2)$$

where I_{tot} is the total aggregated interference, I_i the lognormal components which are summed up, $Y_i \sim N(m_{Y_i}, \sigma_{Y_i}^2)$ gives the lognormal distribution of the components with known mean and variances, and $Z \sim N(m_Z, \sigma_Z^2)$ gives the log-normally distributed approximation. Here,

$$\begin{aligned} m_z &= 2\ln u_1 - \tfrac{1}{2}\ln u_2 \\ \sigma_z^2 &= \ln u_2 - 2\ln u_1. \end{aligned} \tag{2-3}$$

Further,

$$\begin{aligned} u_1 &= \sum_{i=1}^{N} e^{m_{y_i} + \frac{1}{2}\sigma_{y_i}^2} \\ u_2 &= \sum_{i=1}^{N} e^{2m_{y_i} + 2\sigma_{y_i}^2} + \sum_{i=1}^{N-1}\sum_{j=i+1}^{N} e^{m_{y_i} + m_{y_j}} \rho_{i,j} \\ \rho_{i,j} &= e^{\frac{1}{2}\left(\sigma_{y_i}^2 + \sigma_{y_j}^2 + 2r_{ij}\sigma_{y_i}\sigma_{y_j}\right)} \end{aligned} \tag{2-4}$$

where r_{ij} denotes the correlation coefficient

$$r_{ij} = \frac{E\left\{\left(Y_i - m_{y_i}\right)\left(Y_j - m_{y_j}\right)\right\}}{\sigma_{y_i}\sigma_{y_j}} \tag{2-5}$$

The FW approximation e^Z is obtained by simply combining the above equations.

3 Proposed interference models for a database-aided scheme

3.1 Exclusion region model

In this section, we briefly review the mathematical model for the probability distribution of the aggregate interference with exclusion region. It is suitable for describing a situation where a single primary receiver is interfered by many secondary transmitters. The secondary users employ a decision rule by which they make an independent decision whether to transmit or not. Secondary use of radar or aeronautical spectrum by multiple low-power devices can be regarded as a practical example of this model. The description of this section is based on [30][31][32].

3.1.1 Concept of exclusion region

Let us consider a circular area with the radius R where a single primary victim is located at the origin of the circle. Multiple secondary transmitters are randomly distributed in the circle following a Poisson point process with a density λ or uniform distribution with the number of users N. Then, the exclusion region, or no-talk region, is defined inside which the transmission of secondary users is not allowed to avoid detrimental interference to the primary victim. We assume that secondary users have the same transmit power outside the exclusion region.

Consider an arbitrary secondary user j whose distance from the primary user is denoted by a random variable (RV) r_j. We define ξ_j as the interference that the primary user would receive from the user j if it were to transmit. Then, ξ_j is given by

$$\xi_j = GP_{tx}L(r_j)X_j, \tag{3-1}$$

where P_{tx} denotes the transmit power of the secondary user, X_j is a RV modelling fading effect, and $L(r_j)$ is the distance-dependent path loss modelled as $L(r_j) = Cr_j^{-\alpha}$ where C is a constant and α is an exponent. The other gains and losses are accounted for by G. We also define $\tilde{\xi}_j$ as the estimate of ξ_j by the secondary user j. Note that $\xi_j = \tilde{\xi}_j$ only when the secondary user has the perfect knowledge of the propagation loss to the primary victim.

Let I_j be the actual interference from the secondary user j under the exclusion region scheme. Since each secondary user makes an autonomous decision on whether to transmit or not, the decision relies on the estimate of interference to primary victim ($\tilde{\xi}_j$), whereas the amount of interference is ξ_j if it transmits. Thus, I_j is given by

$$I_j = \begin{cases} \xi_j, & \text{if } \tilde{\xi}_j \le I_{thr} \\ 0, & \text{otherwise} \end{cases}, \tag{3-2}$$

where I_{thr} denotes the interference threshold or decision rule applied to each individual secondary user.

Due to the effect of fading, the shape of exclusion region may not be regular. In fact, it depends on the level of knowledge that the secondary users have about the propagation loss to the primary victim. When the secondary users have good knowledge of the propagation (e.g. accurate spectrum sensing is available) the exclusion region becomes irregular to account for the fading effect. On the other hand, if the secondary users have limited knowledge (e.g. they rely on geo-location database where distance-based path loss is only available), a circular exclusion region will be applied. In the latter case, a conservative decision may be needed to compensate the uncertainty on the propagation

environment. Figure 3-1 shows two extreme cases of exclusion region shapes depending on the propagation information.

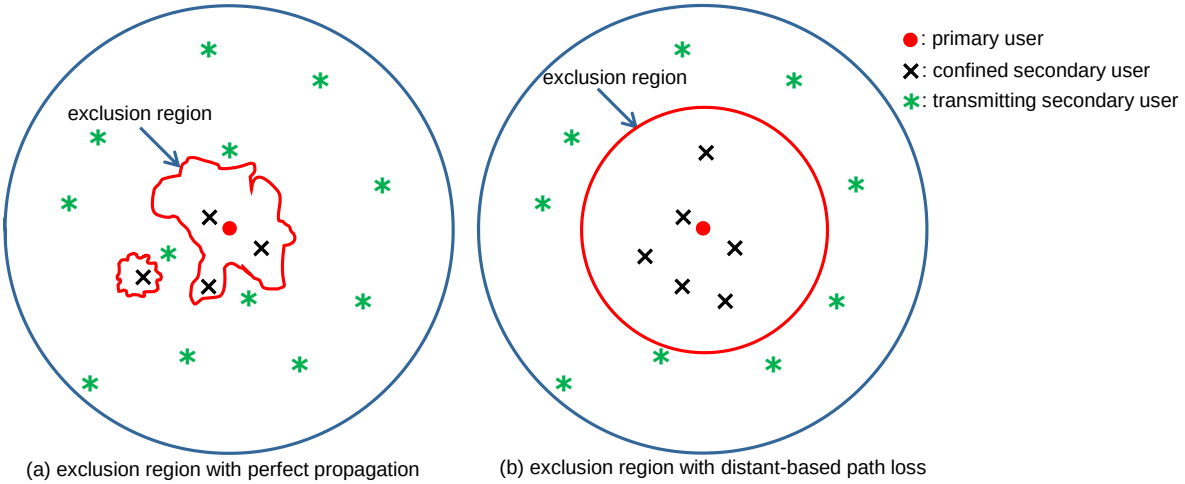

Figure 3-1: Exclusion region shape depending on the propagation knowledge.

3.1.2 **Cumulants of aggregate interference**

The aggregate interference can be expressed as the sum of the individual interference as it is shown below:

$$I_a = \sum_{j\in\Pi_{tx}} I_j = GP_{tx}C \underbrace{\sum_{j\in\Pi_{tx}} r_j^{-\alpha} X_j}_{I_{sum}}, \tag{3-3}$$

where Π_{tx} denotes the set of transmitting secondary users. We assume that the secondary users have perfect propagation knowledge for brevity. The cases with imperfect knowledge will be discussed in detail in Section 4.

Here, we consider two different secondary user distributions. First, we assume that the secondary users are distributed according to a homogeneous Poisson point process with density λ in the annulus[2] of radii $[r_o, R]$. By Campbell's theorem [33], the characteristic function of I_{sum} is given by

$$\Psi_{I_{sum}}(\omega) = \exp\left(-2\pi\lambda \int_X \int_{r_o}^{R} \left[1-\exp\left(j\omega x r^{-\alpha}\right)\right] \mathbf{1}\left(xr^{-\alpha} < I_{thr}\right) f_X(x) r \,\mathrm{d}r \,\mathrm{d}x\right), \tag{3-4}$$

where $\hat{I}_{thr}$ is $I_{thr} = I_{thr}/(GP_{tx}C)$. Then, the nth order cumulant of I_a is obtained as

$$\kappa_n = 2\pi\lambda GP_{tx}C \int_0^{\infty} \int_{r_o}^{R} x^n r^{1-n\alpha} \mathbf{1}\left(xr^{-\alpha} < I_{thr}\right) f_X(x) \,\mathrm{d}r \,\mathrm{d}x\,. \tag{3-5}$$

Closed form of cumulants for various fading distributions can be found in [30][Ghasemi2008].

Second, we assume a special case where the exact number of secondary users is known, which is denoted by N. Further, we consider a RV X_j to model the shadow fading, i.e. secondary users experience shadow fading which follows Gaussian distribution with zero mean and the standard deviation of $\sigma_{X_j}^{dB}$ in dB scale. Then, according to [32], the PDF of ξ_j is derived as

[2] Annulus refers to a ring-shaped geometric figure which is described by two radii, i.e. inner radius and outer radius.

$$f_{\xi_j}(z) = \Omega z^{\frac{-2}{\alpha}-1}\left[1+\mathrm{erf}\left(\frac{\ln(z/Q)-2\sigma_{X_j}^2/\alpha}{\sqrt{2\sigma_{X_j}^2}}\right)\right], \tag{3-6}$$

where $\sigma_{X_j} = \sigma_{X_j}^{dB}\ln(10)/10$, $Q = GP_{tx}L(R)$, and

$$\Omega = \frac{1}{R^2\alpha}\left(\frac{1}{GP_{tx}C}\right)^{\frac{-2}{\alpha}}\exp\left[2\sigma_{X_j}^2/\alpha^2\right]. \tag{3-7}$$

When I_{thr} is applied to the user j, the transmission is not allowed if $\xi_j > I_{thr}$. This means there will be a portion of secondary users who have the zero transmission power. That portion is given by $1-F_{\xi_j}(I_{thr})$, where $F_Y(\cdot)$ denotes the cumulative distribution function (CDF) of a RV Y. Thus, the PDF of I_j is as follows:

$$f_{I_j}(z) = \begin{cases} 1-F_{\xi_j}(I_{thr}), & z=0, \\ f_{\xi_j}(z), & 0<z\le I_{thr}, \\ 0, & \text{otherwise.} \end{cases} \tag{3-8}$$

Cumulants have an attractive property that the nth cumulant of the sum of independent RVs is equal to the sum of the individual nth cumulants. Thus, κ_n is

$$\kappa_n = \sum_{j=1}^{N}\kappa_{n,j}, \tag{3-9}$$

where $\kappa_{n,j}$ denotes the nth cumulant of I_j which can be easily computed from equation (3-8).

3.1.3 **Method of moments for approximating aggregate interference**

The PDF of I_a can be approximated by a known probability distribution by matching the moments obtained from equation (3-5) and (3-9). Several probability distributions have been proposed in the literature, e.g. log-normal distribution [32], shifted log-normal distribution [30], and truncated stable distribution [31]. It is shown in [32] that central limit theorem can be applied only when there are sufficiently large secondary users.

Among those distributions, log-normal distribution provides a good compromise between the simplicity and the accuracy of approximation. The fitting with log-normal distribution shows an accurate match with simulation data particularly in the tail region [34]. By using the first two cumulants of I_a, the PDF of I_a is approximated by the following log-normal distribution:

$$f_{I_a}(z) = \frac{1}{z\sqrt{2\pi\sigma_{I_a}^2}}\exp\left[\frac{-(\ln z-\mu_{I_a})^2}{2\sigma_{I_a}^2}\right], \tag{3-10}$$

where the parameters μ_{I_a} and $\sigma_{I_a}^2$ are obtained from the following equations:

$$\kappa_1 = \exp\left[\mu_{I_a}+\sigma_{I_a}^2/2\right], \tag{3-11}$$

$$\kappa_2 = \left(\exp\left[\sigma_{I_a}^2\right]-1\right)\exp\left[2\mu_{I_a}+\sigma_{I_a}^2\right]. \tag{3-12}$$

3.2 **Spatial power density model**

For a large number of secondary transmitters it may be computationally difficult to calculate the aggregate interference by using direct summation. Instead of considering

each secondary transmitter individually, the secondary transmitters can be grouped together and the aggregate interference can be described as an integral over the secondary deployment area. In this way the generated interference at the primary receivers can be controlled by controlling the spatial power density emitted from the secondary deployment area.

The area-based interference control method introduces a hierarchical approach for transmission power allocation to the secondary devices. The power density allocations to different areas are coupled due to the aggregate interference requirement. Different areas can have different service demands and can be assigned different power densities. Given the allocated power density to an area, the transmission power level allocation inside that area can be delegated to another entity. Such hierarchical power allocation can simplify the database implementation.

Next, we consider a single secondary deployment area and calculate the moments of the aggregate interference as functions of the spatial power density emitted from the area and the area location. The computation is carried out for a cellular system's downlink in Section 3.2.1 and for an ad hoc type of network in Section 3.2.2. In Section 3.2.3 the impact of correlated secondary transmissions is incorporated into the interference model. In Section 3.2.4 we calculate the maximum allowable interference the secondary users can generate at the protection test points of the primary system. The maximum allowable interference is also expressed as a function of the spatial power density. The benefits of the area-based interference model are discussed in Section 3.2.5.

3.2.1 **Interference model for cellular downlink transmissions**

We consider a cellular system with N_{SU} base stations. The generated interference I_i due to the transmission of the i th base station is

$$I_i = P_i \cdot g(r_i) \cdot 10^{\frac{X_i}{10}} \tag{3-13}$$

where r_i is the distance between the i th base station and the point to compute the aggregate interference, $g(r)$ is the mean attenuation at distance separation equal to r and X_i is a random variable used to describe the slow fading effects.

The X_i is assumed to follow the zero mean Gaussian distribution with standard deviation σ_{SU} expressed in dB. The aggregate interference I_{SU} can be computed by summing the interfering powers from each individual transmitter:

$$I_{SU} = \sum_{i=1}^{N_{SU}} I_i. \tag{3-14}$$

The mean aggregate interference is calculated by averaging over the fading distribution:

$$\mathrm{E}\{I_{SU}\} = \sum_{i=1}^{N_{SU}} \mathrm{E}[I_i] = \sum_{i=1}^{N_{SU}} P_i \cdot g(r_i) \cdot \mathrm{E}\{10^{X_i/10}\} = \exp\left(\frac{\sigma_{SU}^2}{2\xi^2}\right) \cdot \sum_{i=1}^{N_{SU}} P_i \cdot g(r_i) \tag{3-15}$$

where $\xi = 10/\ln 10$ is a scaling constant used to convert the received power from the logarithmic domain to the linear domain.

Interestingly, the impact of slow fading on the mean aggregate interference can be described simply by the scaling term $e^{\sigma_{SU}^2/2\xi^2}$. Equation (3-15) considers the exact location for each interfering transmitter. If to assume all secondary transmitters utilize the same power level $P_i = P_{SU}, \forall i$ the spatial power density emitted from the secondary

deployment area is approximately uniform. In that case, the mean interference can be also expressed as an integral over the secondary deployment area S:

$$\mathrm{E}\{I_{SU}\} = P_{SU} \cdot \exp\left(\frac{\sigma_{SU}^2}{2\xi^2}\right) \cdot \sum_{i=1}^{N_{SU}} g(r_i) \approx P_d \cdot \exp\left(\frac{\sigma_{SU}^2}{2\xi^2}\right) \cdot \iint_S g(r) ds \qquad (3\text{-}16)$$

where the transmission power P_{SU} and the power density P_d over the deployment area S are related through $P_{SU} = P_d \cdot A_f$ where A_f is the footprint of one transmitter. The footprint for a cellular base station can be computed as a function of the cell size and the reuse distance.

The validity of the integral approximation in (3-16) will be studied in Section 5.1. In case the uniform power density approximation is not valid, one can split the area S into subareas that have approximately uniform spatial power density. By using the area-based approximation, the precise location of the secondary interferers is not needed in the computation of the mean interference level. The same mean interference can be generated either by few high-powered or by many low-powered secondary transmitters.

The second moment of the aggregate interference by using direct summation can be read as:

$$\mathrm{E}\{I_{SU}^2\} = \sum_{i=1}^{N_{SU}} \sum_{j=1}^{N_{SU}} \mathrm{E}\{I_i \cdot I_j\} = P_{SU}^2 \cdot \sum_{i=1}^{N_{SU}} \sum_{j=1}^{N_{SU}} g(r_i) \cdot g(r_j) \cdot \mathrm{E}\{10^{(X_i + X_j)/10}\} \qquad (3\text{-}17)$$

where the cross-correlation between two zero mean log-normal RV is

$$\mathrm{E}\{10^{(X_i + X_j)/10}\} = \exp\left(\frac{\sigma_i^2 + \sigma_j^2 + 2 \cdot a_{ij} \cdot \sigma_i \cdot \sigma_j}{2\xi^2}\right). \qquad (3\text{-}18)$$

Next, we show how to compute the second moment of the aggregate interference in the absence of shadowing correlation, $a_{ij} = 0, i \neq j$. In our computations it is assumed that the fading samples of different interfering transmitters are drawn from the same zero mean Gaussian distribution, $\sigma_i = \sigma_j = \sigma_{SU}, \forall i, j$.

$$\begin{aligned} \mathrm{E}\{I_{SU}^2\} &= P_{SU}^2 \cdot \sum_{i=1}^{N_{SU}} \sum_{j=1}^{N_{SU}} g(r_i) \cdot g(r_j) \cdot \exp\left(\frac{2\sigma_{SU}^2 + 2\sigma^2 a_{ij}}{2\xi^2}\right) \\ &= P_{SU}^2 \cdot \sum_{i=1}^{N_{SU}} g^2(r_i) \cdot \exp\left(\frac{4\sigma_{SU}^2}{2\xi^2}\right) + P_{SU}^2 \cdot \sum_{i=1}^{N_{SU}} \sum_{j \neq i}^{N_{SU}} g(r_i) \cdot g(r_j) \cdot \exp\left(\frac{\sigma_{SU}^2}{\xi^2}\right) \\ &= P_{SU}^2 \left(\exp\left(\frac{4\sigma_{SU}^2}{2\xi^2}\right) - \exp\left(\frac{\sigma_{SU}^2}{\xi^2}\right)\right) \sum_{i=1}^{N_{SU}} g^2(r_i) + P_{SU}^2 \exp\left(\frac{\sigma_{SU}^2}{\xi^2}\right) \sum_{i=1}^{N_{SU}} \sum_{j=1}^{N_{SU}} g(r_i) g(r_j) \end{aligned} \qquad (3\text{-}19)$$

where a_{ij} stands for the shadowing cross-correlation coefficient between the ith and jth secondary interferer. Similar to equation (3-16), equation (3-19) can be approximated by using integration over the area

$$\mathrm{E}\{I_{SU}^2\} \approx P_d^2 \exp\left(\frac{\sigma_{SU}^2}{\xi^2}\right) \cdot \left(\exp\left(\frac{\sigma_{SU}^2}{\xi^2}\right) - 1\right) A_f \iint_S g^2(r) ds + P_d^2 \exp\left(\frac{\sigma_{SU}^2}{\xi^2}\right) \cdot \left(\iint_S g(r) ds\right)^2 \qquad (3\text{-}20)$$

where

$$A_f \cdot \sum_{i=1}^{N_{SU}} g^2(r_i) \approx \iint_S g^2(r) ds.$$

One can see that the second moment of the aggregate interference depends also on the footprint of secondary transmitters.

3.2.2 **Interference model for randomly located transmitters**

Secondary users that utilize a random access protocol can be modeled by a Poisson point process (PPP). The interference from a single secondary user that is randomly located in the area can be described as an integral over the possible user locations.

$$I_i = P_{SU} \cdot y_i \cdot \iint_S g(r) p_S(s) ds \tag{3-21}$$

where $y_i = 10^{X_i/10}$ follows the log-normal distribution and $p_S(s)$ is the probability of finding the user at the location s. The moment generating function $M_{I_1}(t)$ of the interference distribution due to the transmission of a single secondary user can be read as [20]:

$$M_{I_1}(t) = \int_y p_Y(y) \iint_S \exp\left(t \cdot P_{SU} \cdot g(r) \cdot y\right) p_S(s) ds\, dy \tag{3-22}$$

where $p_Y(y)$ is the log-normal PDF.

According to the PPP model, the interferers are uniformly distributed inside the area, $p_S(s) = 1/S$. The probability of having exactly k independent users active inside the area can be computed from the Poisson PDF:

$$\Pr(k) = \frac{N_{SU}^k \cdot e^{-N_{SU}}}{k!} \tag{3-23}$$

where N_{SU} is the average number of active users in the area.

The moment generating function for the aggregate interference is computed by weighting the conditional moment with the probability of having k active interferers [29]:

$$F(t) = \sum_{k=0}^{\infty} \mathrm{E}\{M(t) \mid k\} \cdot \Pr(k) = \sum_{k=0}^{\infty} \left(M_{I_1}(t)\right)^k \cdot \frac{N_{SU}^k \cdot e^{-N_{SU}}}{k!} = e^{N_{SU} \cdot \left(M_{I_1}(t) - 1\right)}. \tag{3-24}$$

The nth moment of the aggregate interference distribution can be computed from the nth derivative. For $n = 1$:

$$\mathrm{E}\{I_{SU}\} = F'(t)\big|_{t=0} = P_d \cdot \exp\left(\frac{\sigma_{SU}^2}{2\xi^2}\right) \cdot \iint_S g(r) ds \tag{3-25}$$

where it has been used that $M_{I_1}(0) = 1$.

One can notice that the mean interference for the PPP model is the same as for the cellular case (3-16). The second moment for a Poisson field can be computed from the second derivative:

$$\mathrm{E}\{I_{SU}^2\} = F''(t)\big|_{t=0} = P_d^2 \cdot \exp\left(\frac{2\sigma_{SU}^2}{\xi^2}\right) \cdot A_f \cdot \iint_S g^2(r) ds + P_d^2 \cdot \exp\left(\frac{\sigma_{SU}^2}{\xi^2}\right) \cdot \left(\iint_S g(r) ds\right)^2 \tag{3-26}$$

where A_f is the average secondary footprint.

The cellular uncorrelated case and the PPP case are characterized by the same first moment of aggregate interference. Their second moments are described by similar equations. By comparing (3-20) and (3-26) one can see that the PPP has higher second moment. The difference is equal to:

$$P_d^2 \cdot \exp\left(\frac{\sigma_{SU}^2}{\xi^2}\right) \cdot A_f \cdot \iint_S g^2(r) ds. \tag{3-27}$$

3.2.3 **Interference model for correlated secondary transmissions**

The first moment of the aggregate interference does not depend on the correlation of secondary transmissions. For the higher moments of the aggregate interference it is difficult to incorporate the impact of correlation into the integral form. One way to do that is to assume a constant correlation coefficient between any secondary transmission pair, $a_{ij} = a, \forall i, j : i \neq j$. In that case, the correlation coefficient can be taken outside of the summation in (3-19) and the second moment can be expressed in the following integral form:

$$\begin{aligned} \mathrm{E}\left\{I_{SU}^2\right\} \approx\ & P_d^2 \cdot \exp\left(\frac{\sigma_{SU}^2}{\xi^2}\right) \cdot \left(\exp\left(\frac{\sigma_{SU}^2}{\xi^2}\right) - \exp\left(\frac{a\sigma_{SU}^2}{\xi^2}\right)\right) \cdot A_f \cdot \iint_S g^2(r) ds \\ & + P_d^2 \cdot \exp\left(\frac{\sigma_{SU}^2 \cdot (1+a)}{\xi^2}\right) \cdot \left(\iint_S g(r) ds\right)^2. \end{aligned} \tag{3-28}$$

3.2.4 **Interference margin**

In the absence of secondary transmissions the primary receivers may experience the primary system's self-interference. The difference between the self-interference level and the maximum interference level not violating the protection criteria of primary receivers is called the interference margin. The interference margin can be treated as an available resource and the secondary system power allocation can be interpreted as a resource sharing problem. In the following we calculate the interference margin and express it as a function of the spatial power density.

The operation of the primary receivers is considered to be satisfactory if a target SINR Γ_t is satisfied with specific location probability $q = 1 - O$ due to the slow fading:

$$\Pr\left(\frac{S}{I_{SU}} \leq \Gamma_t\right) \leq 1 - q \Rightarrow \Pr\left(S^{(dB)} - I_{SU}^{(dB)} \leq \Gamma_t^{(dB)}\right) \leq 1 - q\,. \tag{3-29}$$

Starting from (3-29) and by using the Cornish-Fischer expansion one can derive the maximum allowable mean generated interference increase in the logarithmic domain that does not violate the operation of primary receivers:

$$\mathrm{E}\left\{I_{SU}^{(dB)}\right\} \leq \mathrm{E}\left\{S^{(dB)}\right\} - \Gamma_t^{(dB)} + x_q \sqrt{\mathrm{var}\left\{S^{(dB)}\right\} + \mathrm{var}\left\{I_{SU}^{(dB)}\right\}} \overset{def}{=} I_\Delta^{(dB)} \tag{3-30}$$

where $I_\Delta^{(dB)}$ is the interference margin in the logarithmic domain.

If the useful signal level $S^{(dB)}$ and the aggregate interference level $I_{SU}^{(dB)}$ are modeled with Gaussian distributions then, $x_q = Q^{-1}(1-q)$ is the q-quantile of a standard Gaussian distribution. The Gaussian approximation for the aggregate interference distribution was shown to be valid when the inter-distances between the interferers are small compared

to the distances between the interferers and the primary test point [44]. The Cornish-Fischer expansion can be utilized to express the interference margin in the form of (3-30) even if the distributions of $S^{(dB)}$ and $I^{(dB)}$ are not Gaussian. In that case, the x_q becomes function of the q-quantiles of the standard Gaussian and of the cumulants of signal level $S^{(dB)}$ and interference level $I_{SU}^{(dB)}$. The bound for interference that guarantees primary system protection can also be derived by using Monte Carlo simulation as suggested in ECC Report 159 [42].

The nuisance parameters not directly expressed in (3-30) like antenna discrimination, polarization and gain can be incorporated into the calculation of the interference margin through some additional parameter M:

$$\mathrm{E}\left\{I_{SU}^{(dB)}\right\} \le \mathrm{E}\left\{S^{(dB)}\right\} - \Gamma_t^{(dB)} + x_q \sqrt{\mathrm{var}\left\{S^{(dB)}\right\} + \mathrm{var}\left\{I_{SU}^{(dB)}\right\}} + M \overset{def}{=} I_{\Delta}^{(dB)}. \tag{3-31}$$

We note that the upper bound on the mean aggregate interference in the log-domain $\mathrm{E}\left\{I^{(dB)}\right\} \le I_{\Delta}^{(dB)}$ also sets a limit for $\mathrm{E}\left\{I_{SU}\right\}$ which is a linear function of the mean received power from the different secondary transmitters. For instance, if the aggregate interference is modelled by the log-normal distribution, we have [47]:

$$\mathrm{E}\left\{I_{SU}\right\} \le \exp\left(\frac{1}{\xi}\cdot\left(I_{\Delta}^{(dB)} + \frac{1}{2\xi}\mathrm{var}\left\{I_{SU}^{(dB)}\right\}\right)\right) \overset{def}{=} I_{\Delta} \tag{3-32}$$

where I_{Δ} is the interference margin in the linear domain.

By combining (3-16) and (3-32) the maximum allowable power density allocated to the secondary deployment area can be read as a function of the interference margin I_{Δ}:

$$P_d \le \exp\left(-\frac{\sigma_{SU}^2}{2\xi^2}\right)\cdot\left(\iint_S g(r)ds\right)^{-1}\cdot I_{\Delta}. \tag{3-33}$$

Usually, there are multiple primary receivers (or primary test points) where the aggregate interference has to be controlled. The condition (3-33) must be satisfied for all these points. The available interference margin can be different at different test points because different points can have different SINR.

As already mentioned, the interference margin can be treated as an available resource. Let us consider the test point p. Each active secondary user is allowed to take a bite, $P_i\, g(r_{ip})$, out of the total available margin $I_{\Delta,p}$:

$$\mathrm{E}\left\{I_{SU_p}\right\} = \sum_{i=1}^{N_{SU}} P_i \cdot g(r_{ip}) \le I_{\Delta,p}\,. \tag{3-34}$$

Let us assume that the secondary deployment area is split into K areas and N_{SU_k} denotes the number of active users belonging to the k th area. The generated interference at the p th test point is:

$$I_{SU_p} = \sum_{i=1}^{N} P_i \cdot g(r_{ip}) = \sum_{k=1}^{K}\sum_{i=1}^{N_{SU_k}} P_k \cdot g(r_{ip}) \tag{3-35}$$

where P_k is the transmission power level for all the users belonging to the k th area.

The secondary users can be grouped based on the similarity of power levels and channel attenuations. The area covered by a group of secondary users is described by the

approximately uniform power density level $P_{d_k} = P_k / A_{f_k}$ where A_{f_k} stands for the average footprint. By using the power density instead of the transmission power level, the generated interference can be read as:

$$I_{SU_p} = \sum_{i=1}^{N} P_i \cdot g(r_{ip}) = \sum_{k=1}^{K} \sum_{i=1}^{N_{SU_k}} P_{d_k} \cdot A_{f_k} \cdot g(r_{kp}) = \sum_{k=1}^{K} P_{d_k} \cdot \int_{S_k} g(r) ds = \sum_{k=1}^{K} P_{d_k} \cdot G_{kp} \quad (3\text{-}36)$$

where the $G_{kp} = \int_{S_k} g_{kp}\, ds$ denotes the propagation loss between the area k and the protection point *p*. In Section 5.3 we will illustrate that the transmissions from secondary users located inside the same area S_k can be correlated.

Equation (3-36) indicates that the allocation of transmission power levels to the secondary users inside a certain area S_k can vary as long as the power density emitted from the area is controlled. Inside an area the allocated interference margin I_{Δ_k} can be taken by few high-powered transmitters or many low-powered transmitters, e.g. small number of base stations or large number of user equipments.

The database can delegate the interference control to different areas simply by allocating in each area a fraction of the interference margin I_{Δ_k} . In that case the sum of allocated interference margins to the areas should not exceed the entire interference margin:

$$\sum_{k=1}^{K} I_{\Delta_k} \leq I_{\Delta}. \quad (3\text{-}37)$$

3.2.5 **Benefits of the power density method**

The benefits of the proposed approach can be described as following

- We can consider aggregate interference from multiple secondary interferers and still guarantee the reception quality of the incumbent receivers.
- Multiple databases can allocate power to secondary users based on the same resource (interference margin at the primary receiver). The power density method along with the concept of interference margin allows multiple databases to make the power allocation independently and still guarantee the reception quality. Each database is allocated the interference resource. The transmission power allocation to secondary users inside the area managed by a database can fill only the interference resource allocated to that database.
- If a database runs off of its allocated interference resource it can negotiate with other database to acquire more resources.
- The spectrum cannot only be allocated to a single secondary transmitter but also it can be allocated to a system that operates in certain area. The interference control is parameterized and those parameters are sent to the system. The interference control could be delegated to the radio resource manager of the system.
- The power allocation can be separated on an area basis. The power allocation in a smaller area than in the whole white space creates a hierarchical power allocation infrastructure. Such infrastructure simplifies the practical database implementation

4 Applications of the exclusion region model

4.1 Incorporating heterogeneous secondary user densities

4.1.1 Motivation

In Section 3.1, we described the basic mathematical models of aggregate interference with exclusion region. It was assumed that the secondary users are distributed in a homogeneous manner over a large area. In practical environments, however, it is usual that the secondary users have heterogeneity in spatial user distribution. For example, let us consider low power secondary users such as WLAN devices. The towns or cities will have higher concentration of secondary users than the rural areas.

In this section, a framework is proposed in order to address the heterogeneity in secondary user distribution. The description of framework is based on [35][36][37]. We consider a situation that there are several zones with different levels of concentration in the whole area of a homogeneous or uniform background user density. Each zone is modeled as an annulus sector, which is termed *hot zone*. The proposed hot zone model has an advantage that various shapes of hot zones can be considered by adjusting the parameters of the annulus sector. We investigate the impact of shaping parameters of the hot zone such as the distance from the primary receiver and size of the hot zone. Note that the hot zone model can be easily applied to the existing aggregate interference models.

4.1.2 Proposed hot zone model

Modeling of heterogeneous secondary user distributions should be done first in order to obtain the PDF of I_a. We can expect various models to describe the heterogeneity depending on specific geographical locations and the types of primary and secondary systems. In this section, we consider a large area consisting of cities, towns, and rural areas. It is usual that the population density of a city or town is much higher than that of rural area. It is also reasonable to consider that the number of secondary users is proportional to the population density. Further, we assume that the secondary users are homogeneously distributed within each city or town with its own density.

We employ an annulus sector, namely hot zone, to describe the crowded region as depicted in Figure 4-1. The idea of using annulus sector is inspired by recent work in the field of secondary spectrum access. In [31], non-circular area is described by the aggregation of infinitesimal annulus sectors. In [38], the impact of secondary field size was investigated by assuming the annulus sector area.

The annulus sector can be molded to various shapes by means of the three shaping parameters: r_H, Δ_{r_H}, and θ_H. As illustrated in Figure 4-1, r_H is the distance between the center of the hot zone and the primary user, the length of the hot zone (depth) is $2\Delta_{r_H}$, and the central angle (width) is given by θ_H. The distance, depth, and width characterize the hot zone along with the density within the zone. We will focus on the description of single hot zone for brevity and for better investigation of its impact on the aggregate interference. Extending our framework to several hot zones with different densities is trivial.

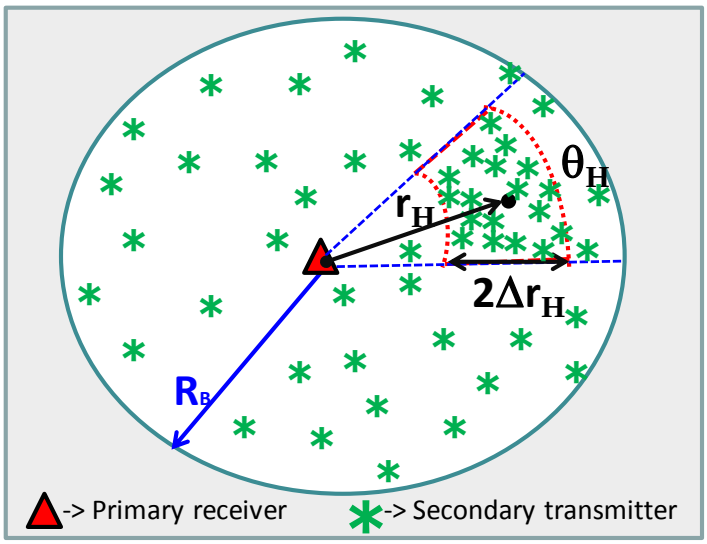

Figure 4-1: Illustration of hot zone model.

The hot zone model is roughly demonstrated in near Stockholm area as depicted in Figure 4-2. Meteorological radar in 5.6 GHz and aeronautical DME transponder in 1 GHz located in Arlanda airport could be considered as potential primary receiver. Then, primary user is about 35 km away from the Stockholm city where population density is significantly higher than surrounding areas.

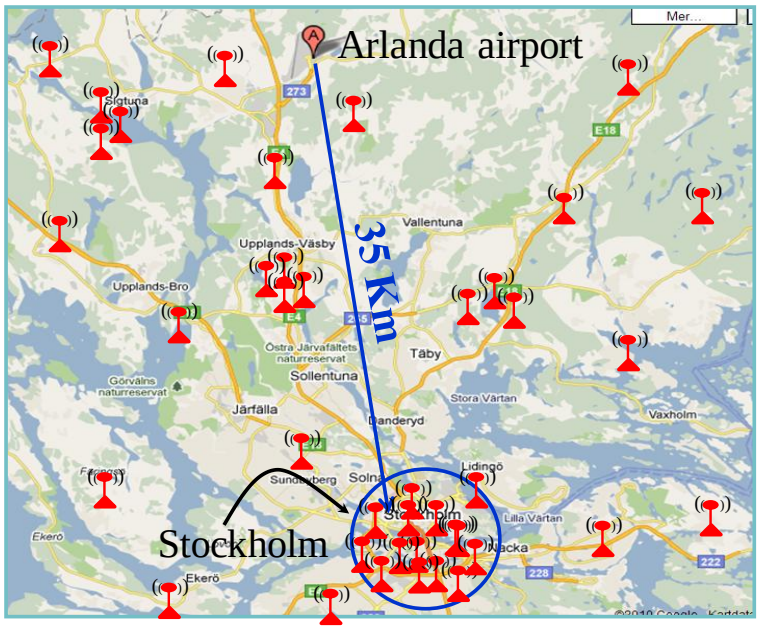

Figure 4-2: Application of hot zone model in Stockholm area; background image taken from Google Maps (http://maps.google.com).

We assume that N_B secondary users are uniformly distributed in a circle of radius R_B (background). Then, N_H secondary users are uniformly overlaid within a hot zone. Let ρ_B and ρ_H denote the densities of secondary users in the background and the hot zone, respectively $(\rho_H > \rho_B)$. Aggregate interference from the background and hot zone are denoted by I_B and I_H, respectively. Total aggregate interference I_a is then

$$I_a = I_B + I_H . \tag{4-1}$$

Let us consider an annulus sector with inner radius R_1, outer radius R_2, and central angle θ_c. It is important that the background circle (as well as hot zone) can be regarded as a special case of the annulus sector. For the case of the background, the following parameters are applied: $R_1 = 0$, $R_2 = R_B$, and $\theta_c = 2\pi$. As for the hot zone, the parameters are $R_1 = r_H - \Delta_{r_H}$, $R_2 = r_H + \Delta_{r_H}$, and $\theta_c = \theta_H$. From the mathematical framework described in Section 3, it is straightforward to derive the cumulants of I_B and I_H. Then, due to the property of the cumulants, the cumulants of I_a can be easily obtained by summing these two cumulants. Similar to homogeneous distributed secondary users, I_a with the hot zone is well described by a log-normal distribution particularly in the tail region.

4.1.3 **Impact of heterogeneous densities on aggregate interference**

The impact of hot zone shaping parameters (r_H and Δ_{r_H}) is presented below. The experimental parameters can be found in [35]. The results are based on the assumption that the secondary users have accurate knowledge of propagation loss ($\xi_j = \tilde{\xi}_j$).

In Figure 4-3, we vary r_H, the distance between the primary receiver and the center of the hot zone, for the two different interference protection requirements. The result is compared with a simple assumption that the same volume of secondary users is uniformly spread in the background. It is observed that the uniform assumption significantly underestimates the aggregate interference when the hot zone is close to the primary receiver and I_{thr} requirement is loose. However, the heterogeneity may not need to be considered if the hot zone is far away from the primary user. When the I_{thr} requirement is tight, the hot zone does not make a visible impact. This is because the most of secondary users close to the primary receiver have to keep silent.

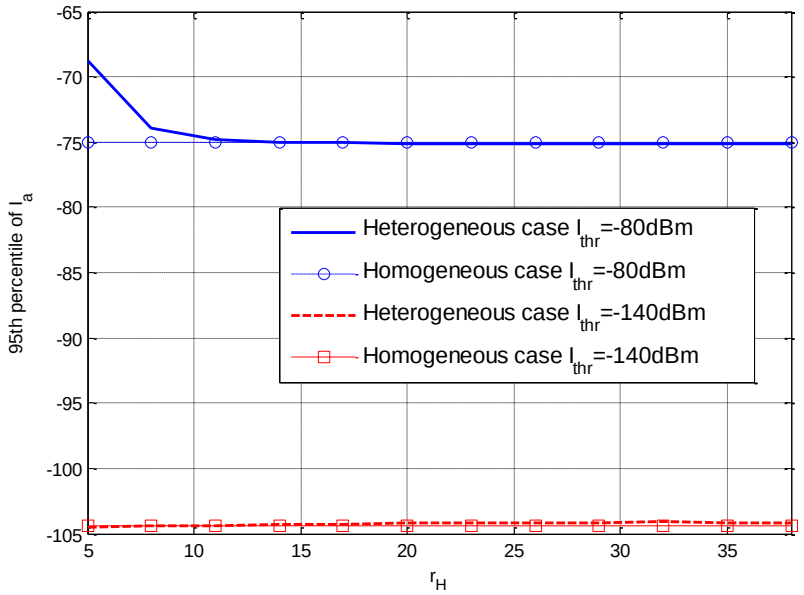

Figure 4-3: Impact of r_H on I_a with the parameters $\Delta_{r_H} = 5\text{km}$, $\rho_B = 1/\text{km}^2$, and $\rho_H = 20/\text{km}^2$.

In Figure 4-4, we experiment with different values of the depth $[r_H - \Delta_{r_H}, r_H + \Delta_{r_H}]$ while keeping r_H fixed. It shows how the depth affects the aggregate interference. If the center of the hot zone is 80km away from the primary receiver, a variation in Δ_{r_H} does not make a noticeable impact on the aggregate interference. The contrary case happens when the center of the hot zone is only 30 km away from the primary user. The

aggregate interference increases with the increment of Δ_{r_H} when $I_{thr} = -80\text{dBm}$ and decreases when $I_{thr} = -140\text{dBm}$. This is because more secondary users are located close to the primary receiver as the hot zone disperses. It causes more interference when they are allowed to transmit ($I_{thr} = -80\text{dBm}$) and less interference otherwise ($I_{thr} = -140\text{dBm}$).

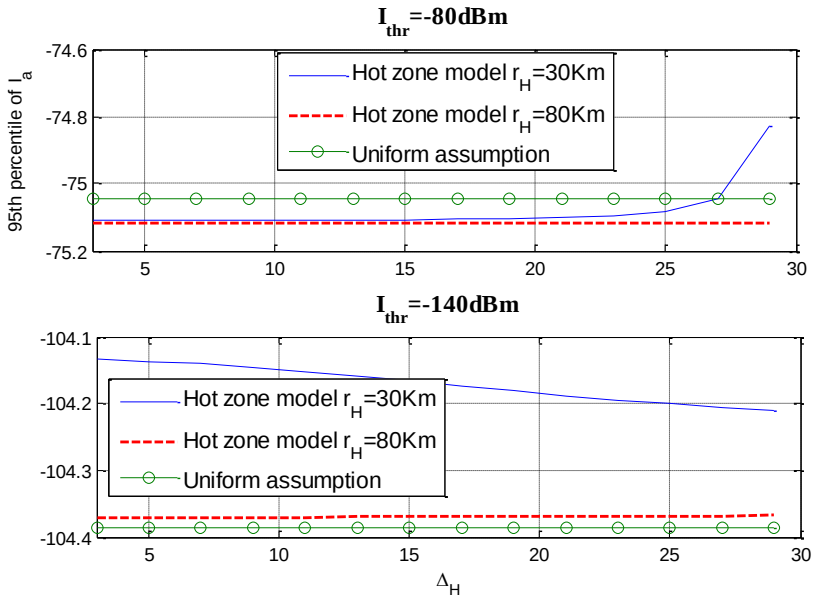

Figure 4-4: Impact of Δ_{r_H} on I_a with $N_H = 1500$ and $\rho_B = 1/\text{km}^2$.

4.2 Aggregate interference in radar spectrum

The basic mathematical framework described in Section 3 can also be utilized to describe the expected aggregate interference to real-life legacy equipment with the minimal modification of the model. In this section, the application of the framework to the radar spectrum is discussed. The discussion here is based on [36] and [37]. Secondary users are low-power indoor devices such as Wi-Fi and femtocell that spread over a large area surrounding the primary victim.

4.2.1 Radar as a potential primary system

Radar accounts for large amount of useful spectrum such as 2.7-3.1 GHz and 5.15-5.75 GHz. Various types of radars are in operation for the purposes of air traffic control, maritime navigation, meteorological aid, and more. Detailed description about technical characteristics of radars can be found in [36][39] and references therein.

From the viewpoint of aggregate interference modeling, the most of radars, particularly those for air traffic control and weather forecast, have the following distinct features. First, spectrum sensing is considered to be a feasible way of primary user detection. Radar relies on the reflection of short radio pulses to examine objects. Thus, receiver is usually collocated with transmitter, and channel reciprocity holds between two paths; one which the secondary user can measure and the other through which it will cause interference to the radar. However, the estimation of propagation loss is only feasible when the basic information about the radar, e.g. EIRP, frequency allocation, is known to the secondary user. It this section, we assume that the secondary users are attached to a central database that feeds the radar information so that they are able to perform a reliable and accurate estimation of propagation loss.

Second, radar employs antenna with high maximum gain (around 30-45 dBi) and sharp beam width. The difference in the path gain between on- and off- main beam is huge.

Therefore, it is secondary users facing the main beam of the radar that makes up significant portion of interference.

Third, the radar antenna rotates in horizontal and/or vertical domain, and it is quite usual that the rotation pattern is regular. This, together with the above feature, means that the secondary users will be able to exploit the temporal access opportunity provided that they have timely and accurate information about the rotation of the radar.

4.2.2 **Aggregate interference to radar**

The antenna pattern of the radar can be simplified as follows:

$$G_{rad} = \begin{cases} G_{\max} & \text{if } 0 \le \theta \le \theta_{MB} \\ 0 & \text{otherwise} \end{cases}, \tag{4-2}$$

where θ_{MB} denotes the main beam width of the radar. Note that the first side lobe of the radar is in the range of 10-20 dBi. Thus, the above simplification should be compensated by using a larger θ_{MB} value than 3dB beam width given in [39].

We assume that each secondary device makes an autonomous decision on whether to transmit or not based on the estimation of interference and the individual interference threshold, as explained in equation (3-2). The estimation of the interference can be divided into the two cases depending on the knowledge of the radar antenna rotation.

Case 1: secondary users are not aware of real-time radar antenna rotation

Since the secondary users do not know the current position of the radar antenna, they have to make a conservative decision that they will create the maximum possible amount of interference, i.e. the radar antenna is facing them. Let ξ_j be the correct expected interference that the secondary user j would cause if it were to transmit. Also, let $\xi_j^{\max}$ be the estimate of ξ_j under the assumption that the user j faces the antenna main beam. Then, the user j does not transmit if $\xi_j^{\max}$ is bigger than I_{thr}. Thus, the interference that the user j creates are expressed as

$$I_j = \begin{cases} \xi_j & \text{if } \xi_j^{\max} \le I_{thr} \\ 0 & \text{otherwise} \end{cases}. \tag{4-3}$$

Case 2: secondary users know exact position of radar antenna

This is rather an optimistic assumption that may hold only when the secondary users are attached to a real-time database that notifies the exact rotation pattern of the radar antenna. In this case, the transmission decision of the secondary user j can be based on the correct estimate of the interference, such that

$$I_j = \begin{cases} \xi_j & \text{if } \xi_j \le I_{thr} \\ 0 & \text{otherwise} \end{cases}. \tag{4-4}$$

Incorporation of equations (4-2) to (4-4) to the framework in Section 3 is simple and straightforward. The areas with and without antenna main beam can be regarded as two separate annulus sectors. Then, the moments of the aggregated interference can be obtained by simply adding the cumulants derived in each of the annulus sectors.

Figure 4-5 illustrates how the required sizes of exclusion regions differ depending on the information about the temporal interference variation. The radar is assumed to be located at the origin of the circle. Fading effects are not considered to obtain a clear graphical representation. The left figure depicts the exclusion region based on equation (4-3). A circular shape of exclusion region is observed since the decisions of secondary users are time-invariant. Entire hot zone is prohibited from transmitting. On the contrary, the right figure, where the exclusion region by equation (4-4) is illustrated, shows a thin line of confined secondary users. Only a part of secondary users in the hot zone is

prohibited from transmitting even when the radar main beam heads towards the hot zone. It shows that the significantly large area can be further utilized by the secondary users if they have exact information about the real-time radar activity. This suggests that the exploitation of temporal opportunity in the radar spectrum is a technique worth investigating although it will be very challenging from the technical perspective.

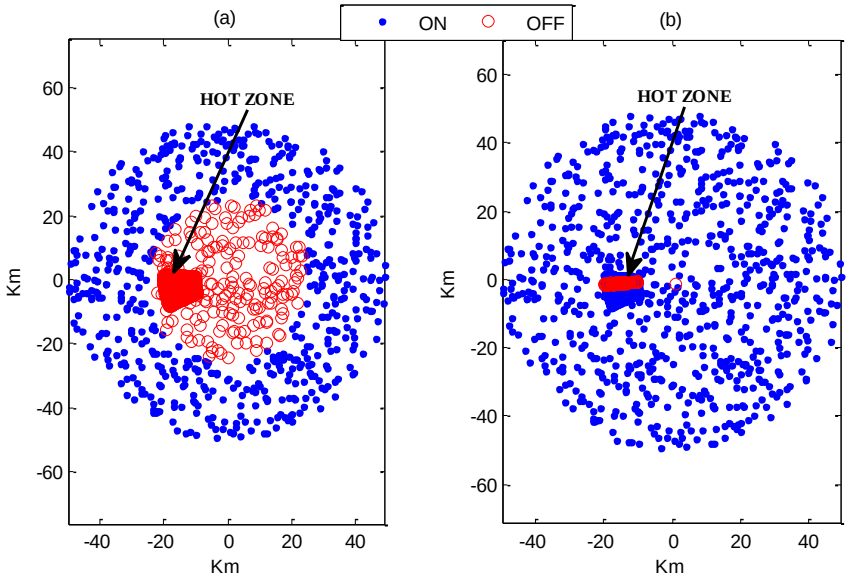

Figure 4-5: Illustration of the exclusive region when secondary users are heterogeneously distributed without fading effects. (a) and (b) represent the case 1 and the case 2, respectively.

4.3 Aggregate interference in aeronautical spectrum

In this section, we demonstrate another example of potential real-life primary system. Distance measuring equipment (DME) for aeronautical navigation is considered to be the primary victim. The discussion is based on [34].

4.3.1 DME as a potential primary system

DME has been in use for aeronautical navigation for more than 50 years. It is operating in 960-1215 MHz. DME is a kind of two-way radar where an interrogator equipped in an aircraft exchanges short Gaussian pulses with a ground transponder to estimate the distance by means of the round trip delay of the radio wave. Detailed description of the DME system can be found in [40]. Let us consider the ground transponder as a potential primary victim. The operation of the transponder is similar to the radar explained in the previous section, but differs from the following aspects: first, it employs omnidirectional antenna in horizontal domain; second, different frequency channels are used for bursting pulses to the interrogator and for receiving signals from the interrogators. The second aspect is important because it may cause an *uncertainty* in the estimation of propagation loss. Notice that the secondary users detect the transponder on the reply (sensing) frequency, while the interference is given on the interrogation (interfering) frequency, which is 63 MHz away from the sensing frequency, as it is shown in Figure 4-6.

In both channels, propagation losses between the DME transponder and the secondary user consist of the distance-based path loss (L) and fading[3] (X and Y). Although it is reasonable to assume that the secondary users accurately estimate the propagation loss of sensing channel ($S=L+X$), it does not necessarily mean that the estimation of interfering channel ($T=L+Y$) is also accurate. Due to the 63 MHz frequency offset between the sensing and interfering channels, *uncertainty* in the estimation of the fading component of the propagation loss between the secondary users and the ground

[3] Note that the fading here refers to the combined effect of shadowing and multi-path fading

transponder still remains. It is overly optimistic to assume that the fading values in these two channels are fully correlated.

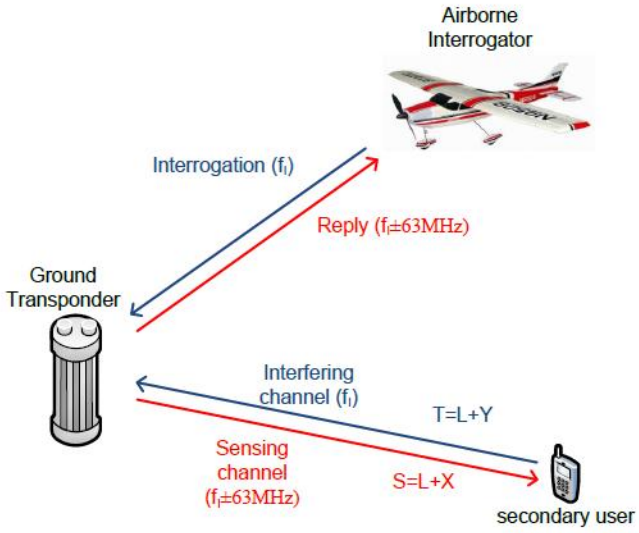

Figure 4-6: Uncertainty in secondary sharing with ground transponder as primary victim

Partial correlation between channels does not allow the secondary user to perfectly estimate its interference to the primary victim. Different levels of *uncertainty* in fading estimation are represented by a correlation coefficient ρ. In the next section, the mathematical framework proposed in [30][31][32] is modified to account for the *uncertainty* in the fading estimation.

4.3.2 **Aggregate interference under fading uncertainty**

We apply the concept of exclusion region described in Section 3.1.1. However, since the secondary user does not have perfect knowledge of the propagation loss to the primary victim, then $\xi_j \neq \tilde{\xi}_j$. Hence, the estimate of ξ_j by the secondary user j $\left(\tilde{\xi}_j\right)$ is given by

$$\tilde{\xi}_j = GP_{tx}L(r_j)X_j, \tag{4-5}$$

where X_j is the RV modelling the fading effect in the reply (sensing) frequency. It is generally considered that the fading consists of shadow fading following a normal distribution in dB scale and multi-path fading by which the instantaneous power is varied with an exponential distribution. We employ an assumption that the composite fading Y_j and X_j follows a log-normal distribution. It is known that this assumption works well when the standard deviation of shadowing is higher than 6 dB, i.e. when the shadowing is a dominant factor of the composite fading [41]. The RV modelling the fading effect in the interrogation (interfering) channel, Y_j, is also modelled as a log-normally distributed random variable whose parameters are the same as X_j.

Since the fading effects in both sensing and interfering channels are modelled as log-normal distributed random variables, the joint distribution of X and Y is given by the following bivariate log-normal distribution:

$$f_{X_j,Y_j}(x,y) = \frac{1}{2\pi xy\sigma^2\sqrt{1-\rho^2}} e^{-\frac{(\ln x)^2 - 2\rho(\ln x)(\ln y) + (\ln y)^2}{2\sigma^2(1-\rho^2)}}, \tag{4-6}$$

where ρ is the correlation coefficient of X and Y:

$$\rho = \frac{Cov(\ln X, \ln Y)}{\sqrt{Var(\ln X)Var(\ln Y)}}, \quad (4\text{-}7)$$

It is expected that shadowing components are closely correlated with each other because the 63 MHz offset will not make a noticeable difference in diffraction characteristics of radio waves. On the other hand, the multi-path fading is considered to be independent with the frequency offset. Thus, it is apparent that the composite fading values, X and Y, are partially correlated $(0<\rho<1)$. Exact value of ρ depends on propagation environments. In this work, we provide a general framework that can take into account the impact of different ρ values.

To obtain the PDF of the aggregate interference I_a, we employ the cumulant-based approximation described in Section 3.1.2. The aggregate interference I_a is calculated according to the equation (3-3). By applying the Campbell's theorem, the characteristic function of I_{sum} is as follows:

$$\Psi_{I_{sum}}(\omega) = \exp\left(-2\pi\lambda \int_X \int_Y \int_{r_o}^{R} \left[1-\exp\left(j\omega y r^{-\alpha}\right)\right] \mathbf{1}\left(r^{-\alpha} x < I_{thr}\right) f_{X,Y}(x,y) r \,\mathrm{d}r \,\mathrm{d}y \,\mathrm{d}x\right), \quad (4\text{-}8)$$

where $\hat{I}_{thr}$ is $I_{thr}=I_{thr}/(GP_{tx}C)$. Then, the nth order cumulant of I_{sum} when there is partial correlation is obtained as

$$\begin{aligned}\kappa_n &= 2\pi\lambda \int_0^{\infty}\int_0^{\infty}\int_{r_o}^{R} x^n r^{1-n\alpha} \mathbf{1}\left(x r^{-\alpha} < I_{thr}\right) f_{X,Y}(x,y)\,\mathrm{d}r\,\mathrm{d}y\,\mathrm{d}x \\ &= \frac{2\pi\lambda}{n\alpha-2}\Bigg[(r_o^{2-n\alpha} - R^{2-n\alpha}) \int_0^{\infty}\int_0^{r_o^{\alpha} I_{thr}} y^n f_{X,Y}(x,y)\mathrm{d}y\mathrm{d}x \\ &\qquad + ((x/I_{thr})^{\frac{(2-n\alpha)}{\alpha}} - R^{2-n\alpha}) \int_0^{\infty}\int_{r_o^{\alpha} I_{thr}}^{R^{\alpha} I_{thr}} y^n f_{X,Y}(x,y)\mathrm{d}y\mathrm{d}x\Bigg]\end{aligned} \quad (4\text{-}9)$$

By inserting equation (4-6) in equation (4-9), we obtain the cumulant of I_{sum} for partial correlation when X_j and Y_j are log-normal variables. Using the cumulant of I_{sum}, the nth order cumulant of the aggregate interference I_a is calculated as follows:

$$k_{I_a}(n) = (GP_{tx}C)^n k_n. \quad (4\text{-}10)$$

By using the first two cumulants of I_a, the pdf of I_a is approximated by the method of moments described in Section 3.1.3.

In Figure 4-7, we show a comparison between the analytical CDF of the I_a calculated by using the cumulate-based approximation and simulation-based CDF of the I_a. A good agreement both CDFs is shown when $\rho > 0$. However, when the fading estimated in the sensing channel is uncorrelated to the fading in the interfering channel, analytical CDF only matches the tails of the simulation-based CDF. Since the main interest lies on the tails of the CDF, this framework is still applicable when $\rho = 0$.

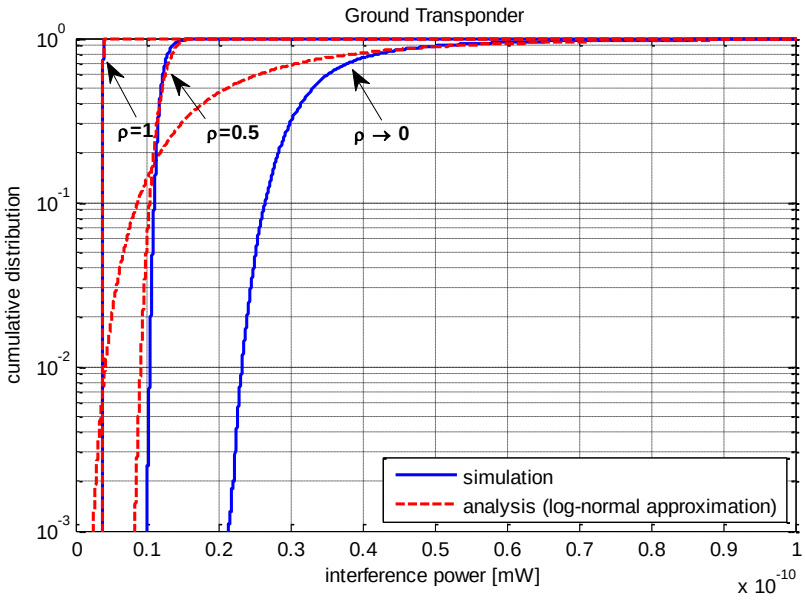

Figure 4-7: A comparison between the analytic CDF of I_a and the result of Monte Carlo simulation; primary receiver is the DME ground transponder ($I_{thr} = -150$ dBm and $\lambda_{SU} = 20/\text{km}^2$)

5 Applications of the spatial power density model in the TV spectrum

In this section we verify that the power density is sufficient for the computation of the aggregate interference in the TV white spaces (TVWS). In Section 5.1 a single secondary area is considered. Also, it is assumed that all secondary transmissions are described by the same channel model $g(r) \sim r^{-\alpha}$. We compute the first two moments of the aggregate interference distribution by using integration and direct summation. Essentially, the integral approximations introduced in equation (3-16) and equation (3-20) are verified. It is shown that for relatively many secondary transmitters the power density can predict accurately the first two moments of the aggregate interference.

In Section 5.2 we use the power density model to set the transmission power level at the secondary transmitters. It is assumed that the aggregate interference follows the log-normal distribution and subsequently equation (3-32) and equation (3-33) can be utilized. The Gaussian approximation for the aggregate interference is verified against Monte Carlo simulations. In Section 5.3 the terrain morphology is taken into consideration and the Longley-Rice model is used to estimate the secondary path loss to the TV test points. It is shown that nearby located transmitters have highly correlated path loss values to the TV test points and subsequently they can be clumped together.

In Section 5.4 the power density method is compared to the current ECC approach for secondary power allocation. It is shown that the ECC approach may violate the TV protection criteria while the power density approach has built-in interference control. In addition, the power density approach may result in higher transmission power levels. In Section 5.5, unlike the current approaches by ECC and FCC, a power allocation method is proposed that considers also the self-interference in the secondary system.

Finally, in Section 5.6 it is shown how to incorporate the non-uniform population density into the interference computation process. It is shown that a homogeneous PPP is not sufficient to describe the aggregate interference distribution. However, a clustered PPP with relatively few clusters is able to capture the impact of non-uniform user density.

5.1 Validate the model for secondary operation in TV spectrum

We show that the power density emitted from the secondary deployment area is sufficient parameter to describe the generated interference at the TV cell border unless the number of secondary transmitters is small. For that, we compute the moments of the aggregate interference by using integration over the area and direct summation. The validation is carried out for a cellular secondary system downlink deployed outside the protection area of a TV transmitter (see Figure 5-1). The channel model for all base stations is the same: $g(r_i) = r_i^{-\alpha_{SU}}$, where α_{SU} is the propagation path loss exponent.

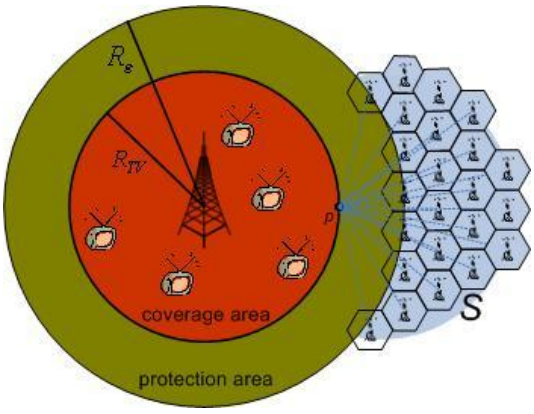

Figure 5-1: Secondary deployment area S outside the circular TV protection area.

Since the geometry of the system is simple, we can identify the TV test point where the aggregate interference is maximized (see Figure 5-1, point p). The parameter settings for the cellular system are summarized in Table 5-1 respectively.

Table 5-1: Parameter settings for the cellular system.

Cellular system	
Locations	Circular deployment area with center at [150 0] km and radius equal to 35 km
Transmission power	For constant power density over the secondary deployment area, the transmission power of the cellular BS varies for different secondary cell size. The cell size will be a parameter in our computations.
Path loss model	Power law based attenuation with path loss exponent $\alpha_{SU} = 3.5$. The standard deviation of the secondary field strength inside a TV test pixel is $\sigma_{SU} = 5.5$ dB.

5.1.1 **Independent shadowing**

In Figure 5-2 we plot the first two moments of the aggregate interference by using integration (equation (3-16) for the mean, equation (3-20) for the second moment) and summation (equation (3-15) for the mean, equation (3-19) for the second moment). The integration is carried out in polar coordinates by using the method proposed in [49]. The transmission power for all secondary base stations is the same and subsequently the emitted spatial power density from the area S is approximately uniform. The integral approximation is validated for three different power density values $P_d = \{100, 300, 500\}$ mW/km^2. For 1 km cell radius and reuse distance 1, these power density values correspond to transmission power levels $P_{SU} = \{0.26, 0.78, 1.3\}$ W.

For small cell size (up to 4 km) the integral approximation is good. For larger cell sizes, the number of secondary base stations reduces and the direct summation is not computationally expensive. For increasing cell sizes the mean aggregate interference increases. The reason being that, the secondary base stations generating most of the interference are located always at the protection area border (see Figure 5-1).

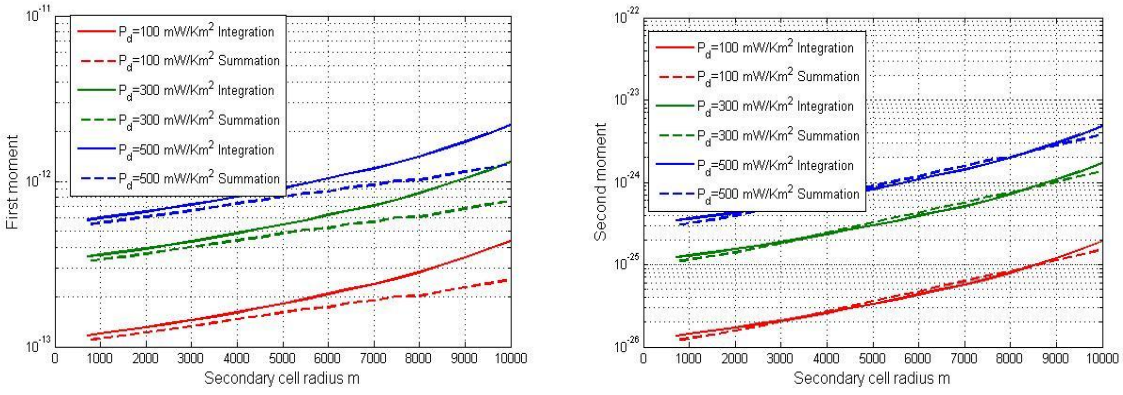

Figure 5-2: Mean aggregate interference level by using integration and summation for different power density values. First moment (left), second moment (right).

5.1.2 **Correlated shadowing**

Measurements indicate that the radio signals arriving from the same angular direction are correlated. The signals arriving from the same direction pass the same large objects. There are various models that describe the slow fading correlation as a function of the signal arrival angle and the relative distance between the interfering transmitters and

the victim receiver [50]-[53]. The slow fading correlation between interfering secondary transmitters will impact the distribution of the generated interference.

As mentioned in Section 3.2.3 the first moment of the aggregate interference for independent and correlated shadowing is the same. The correlation impacts the higher moments of aggregate interference. We use constant correlation coefficient between all pairs of secondary base stations and compare the second moment of the aggregate interference by using integration and direct summation. The results are illustrated in Figure 5-3 where the power density has been taken equal to 385 mW/km^2.

As a general remark, the correlation increases the value of the second moment. The maximum value occurs for fully correlated transmissions. For a large cell size, the integral-based method is not suitable to describe the aggregate interference under correlated shadowing.

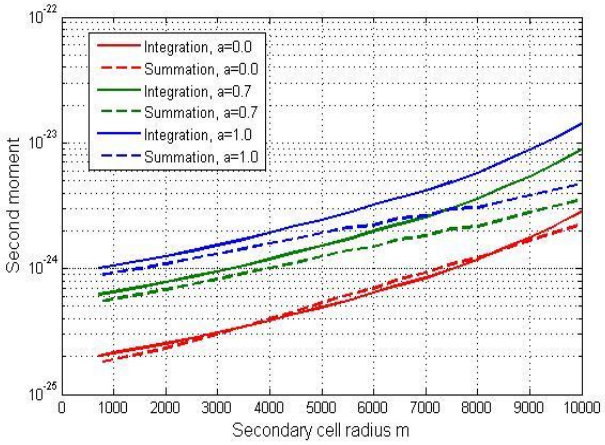

Figure 5-3: Second moment of the aggregate interference by using integration and summation for different power density values. The correlation coefficient is assumed to be the same for all pairs of secondary transmitters. Three values are tested, a={0, 0.7 1}.

5.2 Allocating the spatial power density for single area

In equation (3-33) the maximum permitted power density is calculated by using integral approximation and assuming that the aggregate interference follows the log-normal distribution. In order to validate these two assumptions we compute the maximum permitted power density also by carrying out Monte Carlo simulations.

Recall that the power density is a function of the interference margin at the TV test points. For computing the available margin the protection criteria for the TV system are required. The parameter settings for the TV system are summarized in Table 5-2.

Table 5-2: Parameters settings for the TV system.

TV transmitter	
Locations	[0 0]
Transmission powers	200 kW
Coverage area	140 km
Path loss model	Power law based attenuation with path loss exponent equal to -3.2. The standard deviation of the TV field strength inside a TV test pixel is taken equal to 5.5 dB
Target SINR	$\Gamma_t = 16.5$ dB

Noise level	$P_N = 2.4\ 10^{-14}$ W
Outage probability	$O_{TV} = 0.1$
Protection distance	10 km

5.2.1 **Using analytical interference modeling**

According to (3-30) the interference margin depends on the locations of the secondary base stations through the parameter $\mathrm{var}\left\{I_{SU}^{(dB)}\right\}$. In that case an iterative process would be required to find the secondary transmission power levels eating the entire interference margin. A lower bound on the interference margin that is independent of the secondary locations has been derived in [47] and validated in QUASAR D3.2. It is equal to:

$$I_\Delta \approx \exp\left(Q^{-1}\left(1-O_{TV}\right)\cdot\frac{\sigma_{TV}}{\xi} - \ln\left(\Gamma_t\right) + \frac{M_{TV}}{\xi}\right) - P_N \qquad (5\text{-}1)$$

where M_{TV} is the TV signal level in dB at the test point p.

With the interference margin at hand, we can compute the common transmission power level $P_{SU}^{(A)}$ for all secondary users based on equation (3-33):

$$P_{SU}^{(A)} = \exp\left(-\frac{\sigma_{SU}^2}{2\xi^2}\right)\cdot I_\Delta \cdot A_f \cdot \left(\iint_S r^{-\alpha_{SU}} ds\right)^{-1} \qquad (5\text{-}2)$$

where the integral can be evaluated numerically and the I_Δ is given in (5-1).

5.2.2 **Using Monte Carlo simulations**

For secondary users arranged as a cellular network downlink we cover the secondary deployment area with hexagonal lattice and the users are placed in the centre of the hexagons. It is assumed that the centre of the secondary deployment area lies at the centre of a cell. Let us call this cell by "middle cell". The following steps are carried out in each simulation run.

- The centre of the secondary deployment area is selected randomly within the area of the "middle cell".
- We set the transmission power $P_{SU}^{(MC)}$ equal to $P_{SU}^{(A)}$ for all secondary users.
- We generate 30 000 wanted TV signal power samples at each test pixel. The mean value is M_{TV} and the standard deviation is σ_{TV}.
- We generate 30 000 noise power samples with zero mean and standard deviation equal to the noise power level P_N.
- We generate 30 000 power samples from each secondary user at the test pixel. The values are generated based on the cellular channel model (see Table 5-1).
- For each trial we compute the SINR.
- We calculate the location probability as the ratio of the number of trials where the SINR is larger than the SINR target Γ_t.
- If the location probability is higher than the location probability target we increment the transmission power for all secondary users: $P_{SU}^{(MC)} + \Delta P_{SU}$.

- If the location probability is lower than the location probability target we decrement the transmission power for all secondary users: $P_{SU}^{(MC)} - \Delta P_{SU}$.
- If the location probability is equal to the location probability target we store the value $P_{SU}^{(MC)}$ and stop

In different Monte Carlo simulation runs the same procedure is followed.

Compared to the cellular case downlink, the cellular case uplink is different only in the first step: We allocate randomly 1 secondary user inside each cell.

The comparison of the maximum allowable transmission power is depicted in following two figures for cellular downlink and cellular uplink case. One can see that the mean interference will be lower by using the integral-based method along with the lower bound of the interference margin.

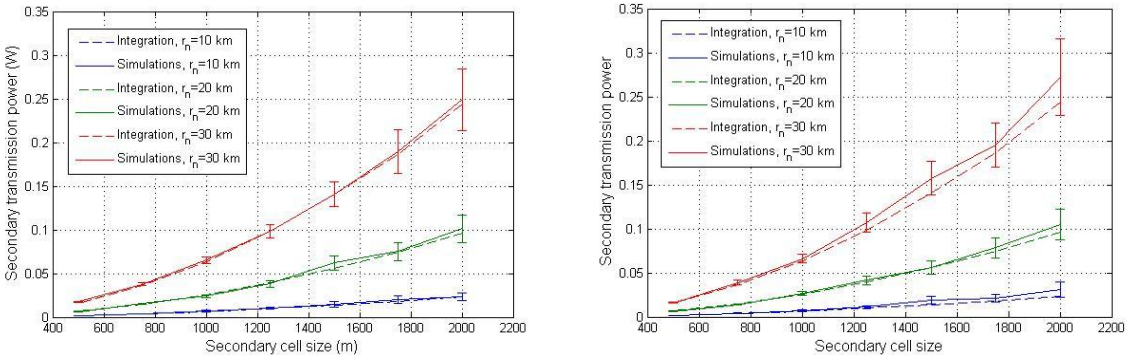

Figure 5-4: The spatial power density calculated by analytical interference modelling is compared to the simulation results. The bars describe the standard deviation of the simulation results. Cellular downlink case (left), cellular uplink case (right).

5.3 Incorporating the impact of the terrain

So far, the power density approximation method has been validated with a simple channel model incorporating power law based attenuation and slow fading. We noticed that the area where the aggregate interference is computed should contain relatively many secondary transmitters and the channel model should not change. In reality, the propagation path loss is affected due to obstruction, scattering, etc. and more complex channel models have been used to account for these phenomena. In a complex environment the power density may not be sufficient for describing the interference generated from the area.

Next, we test the proposed power density approximation method in a realistic environment. In our study we utilize the Longley-Rice propagation model [28] (also known as irregular terrain model ITM) implemented in splat! [45] along with the ground elevation information data [46]. As expected, neighbouring secondary transmitters are attenuated by the same obstacles and have similar path loss values to the TV test points. Because of that, neighbouring transmitters can be grouped together. The database can control the aggregate interference by controlling the emitted power density from each group of secondary transmitters.

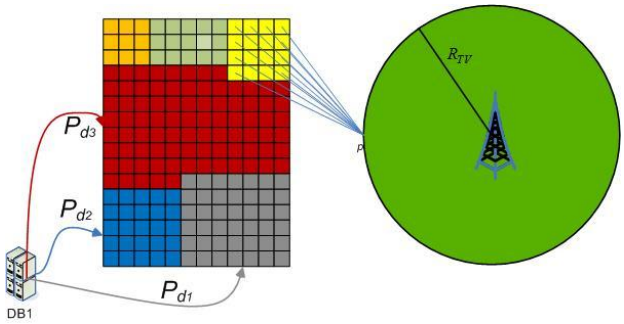

Figure 5-5: Secondary deployment area outside the TV protection contour is split into multiple regions. The spatial power density emitted from a region is sufficient to describe the aggregate interference. The secondary pixels belonging to the same region have the same colour and they experience correlated pathloss values to the TV test points. The database allocates the power density to the multiple regions such that the interference margin at the TV test points is not violated.

5.3.1 **Case study: flat area**

In the first case study, we select a relative flat area in the western part of Finland (see Figure 5-6). The transmission power of MUX-B VAASA TV transmitter is 10 kW and the operational frequency is 602 MHz. The coverage area border of the TV transmitter is defined by the minimum required field strength that is equal to 54.1 dBuV/m at this frequency. The desired to undesired ratio $\Gamma_t^{(dB)}$ is taken equal to 15 dB and should be satisfied with location probability $q = 90$ %.

The secondary deployment area is the blue rectangular area in Figure 5-6 (left). In Figure 5-6 (right) the ground elevation of the secondary area is depicted. The area is divided into rectangular pixels with dimensions 134 x 150 m^2. In total, 150000 pixels are approximately needed to cover the secondary area.

Note that the Longley-Rice propagation model might result in discontinuous TV coverage area. Therefore it is not straightforward to identify the TV test point that will experience the highest aggregate interference as in Section 5.1. Due to the large amount of computations only twenty points of the TV coverage area are selected as the test points. The points that are located closest to the secondary area are likely to experience the highest secondary interference and they are selected to be the test points. The elevation of the TV test points lies between 40 m and 50 m above the ground.

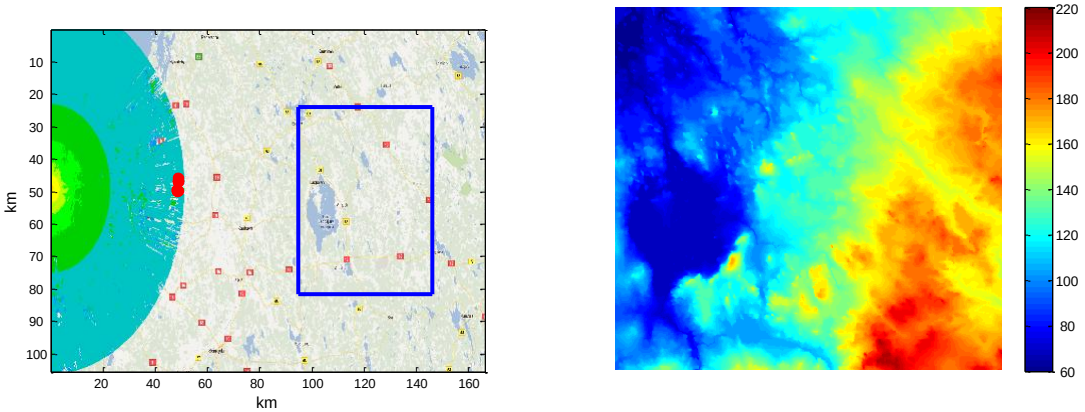

Figure 5-6: Part of the coverage area for MUX-B VAASA TV transmitter in Finland, TV test points and rectangular secondary area (left) and ground elevation for the secondary deployment area (right).

In order to decide whether neighbouring pixels can be grouped together the following heuristic algorithm is used:

- Initially we consider the full secondary area as a cluster.
- For each cluster we compute the maximum permitted power density by using integration (3-33) such that the TV protection constraints are not violated. Then, we carry out Monte Carlo simulations:
    - If the mean power density over the Monte Carlo runs is less than the power density computed by integration the cluster is not further subdivided. The mean power density and its variance are stored and used to characterize the aggregate interference generated from that cluster.
    - If the mean power density over the Monte Carlo runs is higher than the power density computed by integration, the area is subdivided into four equally-sized clusters
- The previous step is repeated for each new generated cluster.

The separation of secondary deployment area into clusters is depicted in Figure 5-7. The resulting clusters in the lower-right corner are large. The pixels at the lower-right corner of the secondary deployment area have clear line-of-sight to the TV test points. Because of that, the WSD transmissions originated from those pixels will be highly correlated. This is illustrated in Figure 5-8.

The secondary deployment area is split into 16 clusters Figure 5-8 (left) and 64 clusters Figure 5-8 (right). The average cross correlation coefficient for the path loss values belonging to the same cluster is computed. By comparing Figure 5-7 and Figure 5-8, one can see that pixels characterized by high correlation form clusters. For instance, the secondary transmissions originated from pixels located in the lower-right corner of the area are indeed highly correlated.

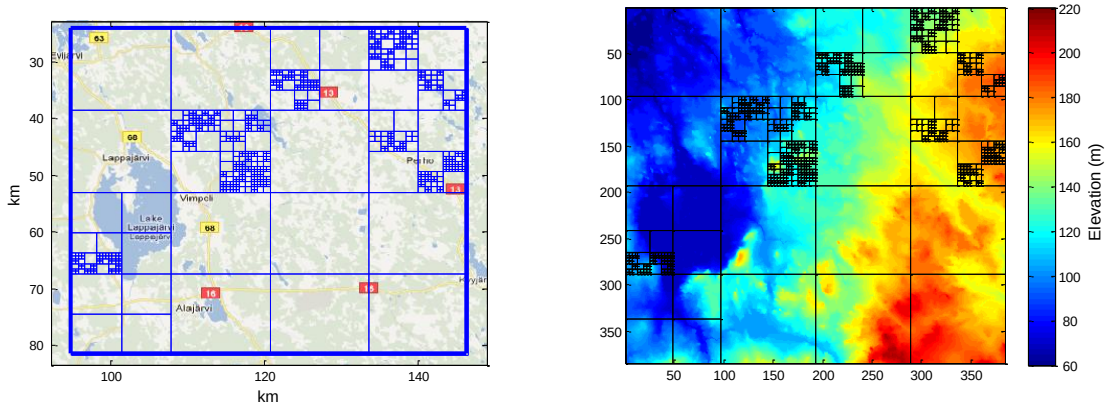

Figure 5-7: Pixels to be used by the database drawn on the top of Google maps (left), ground elevation secondary map (right). Inside each pixel, the emitted spatial power density is sufficient to describe the aggregate interference at the TV test points.

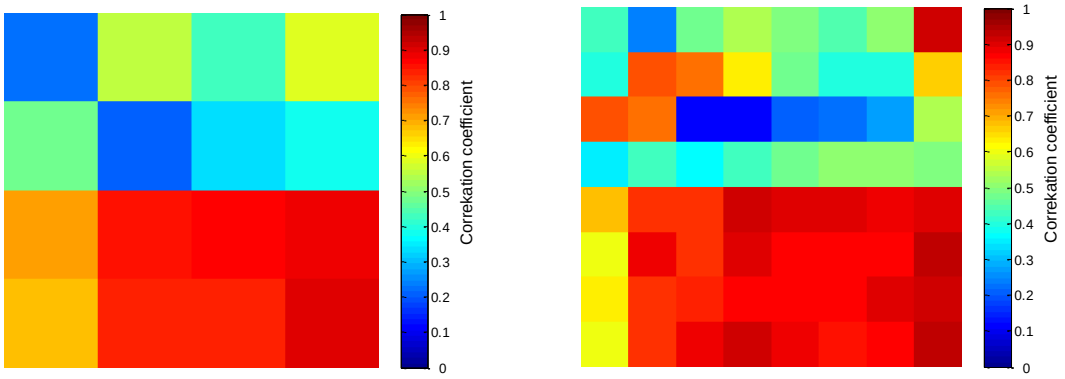

Figure 5-8: Average cross correlation coefficient for secondary transmitters located inside rectangular regions of dimensions 12.8 x 14.4 km² (left) and 6.4 x 7.2 km² (right).

So far it has been illustrated there is a potential to facilitate interference control by splitting the secondary deployment area in clusters that are significantly larger compared to the pixel size. The generated interference from secondary transmitters located in a cluster can be accurately described by the spatial power density. Next, it is shown that the generated interference at the TV test points due to the secondary transmissions belonging to the same region do not violate the protection criteria of TV receivers. In Figure 5-9 the SIR distribution at the TV test points is depicted assuming that each region exists alone and it is allocated the entire available interference margin.

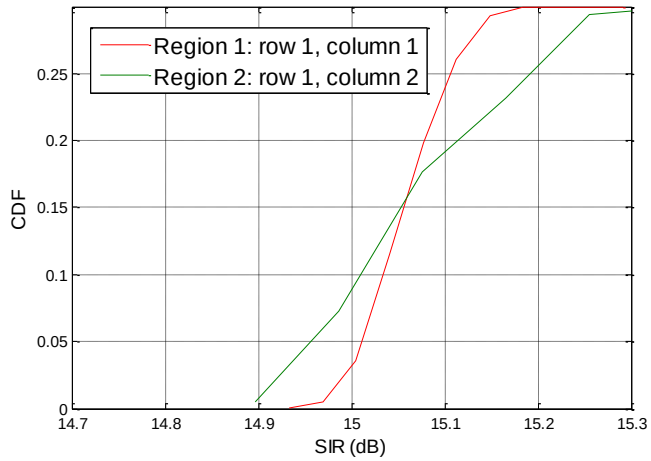

Figure 5-9: SIR distribution at the TV test points due to the transmission originated from the two regions at the upper-left corner of Figure 5-7(left). The allocated power density to region 1 and region 2 is equal to 0.0070 W/km² and 0.0291 W/km² respectively.

5.3.2 **Case study: hilly area**

A similar study is now carried out in a hillier area in Jyväskylä in Finland. The transmission power of the Vihtavuori TV transmitter is 100 W and the operational frequency is 546MHz. At this frequency the minimum required TV field strength is 53.3 dBuV/m. The secondary deployment area has rectangular shape and it is split into pixels with dimensions 140 x 126 m². For a system illustration see Figure 5-10.

In Figure 5-11 the resulting regions in the secondary deployment area are depicted. One can see that the required number of regions to cover approximately the same area size as in previous case study is larger. The reason being, that the secondary deployment area is now hillier. Close to the centre of the deployment area, pixels that are located at a distance of few kilometres from each other have a high difference in ground elevation

and because of that their path loss to the TV test points is characterized by low correlation (see Figure 5-12). Therefore only few neighbouring pixels can be grouped together and the resulting size of the cluster is in the order of square kilometre.

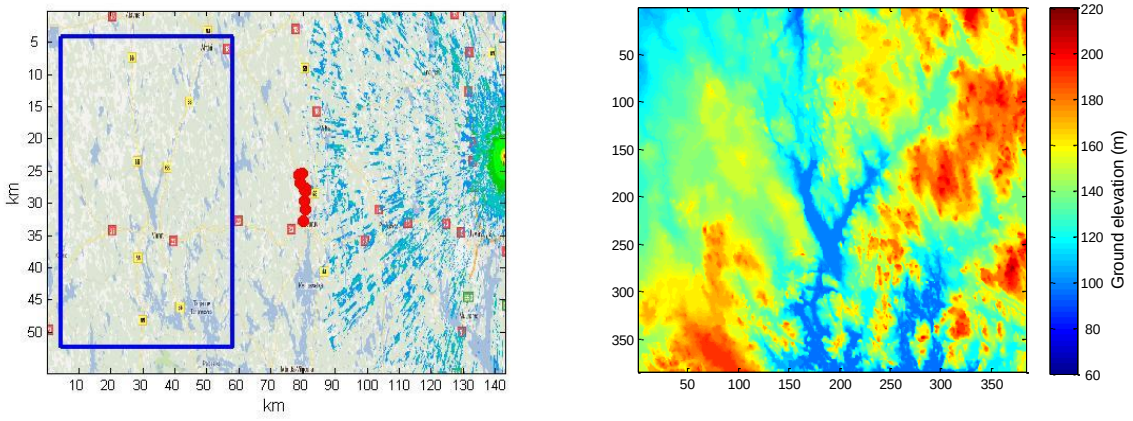

Figure 5-10: Part of the coverage area of Vihtavuori TV transmitter in Finland, TV test points and rectangular secondary area (left), ground elevation for secondary deployment area (right)

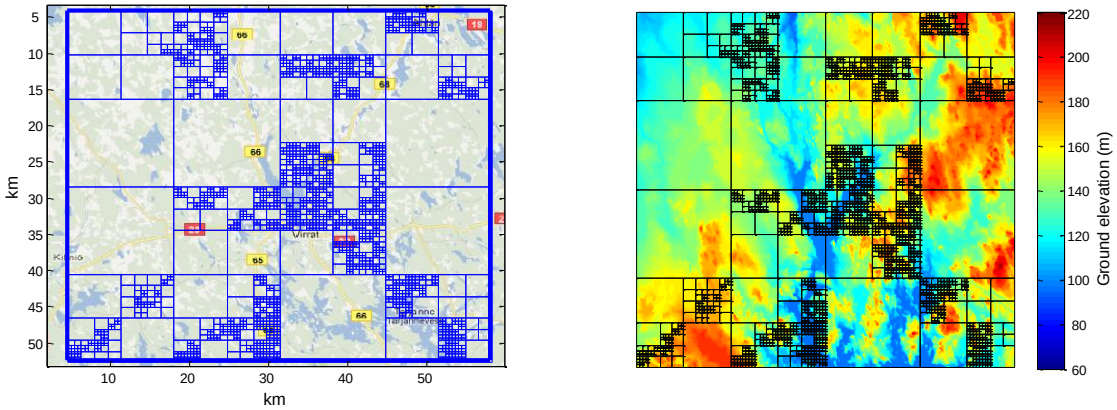

Figure 5-11: Pixels to be used by the database drawn on the top of Google maps (left), ground elevation secondary map (right). Inside each pixel, the emitted spatial power density is sufficient to describe the aggregate interference at the TV test points.

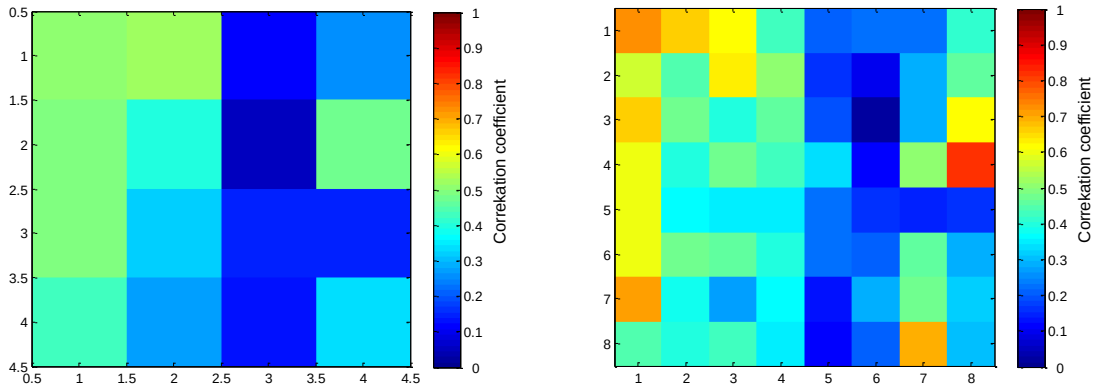

Figure 5-12: Average cross correlation coefficient for secondary transmitters located inside rectangular regions of dimensions 13.4 x 12.1 km² (left) and 6.7 x 6 km² (right).

5.3.3 **Fading correlations**

The impact of shadowing correlation on the aggregate interference has been illustrated in Section 5.1.2 for constant correlation coefficient. In this Section, we illustrate the impact of shadowing correlation on the distribution of the aggregate interference when the terrain data is considered. In Figure 5-13 we depict two different scenarios of secondary deployments. One corresponds to independent transmissions and the other to correlated transmissions. In Figure 5-13 (left) the secondary transmitters are placed far from each other and because of that, their signals does not experience attenuation due to the same obstacles. In Figure 5-13 (right), the secondary transmitters are relatively near to each other and their transmissions are expected to be highly correlated. On average, the distances of the secondary transmitters to the TV test points are equal for the two scenarios. Therefore the difference in the aggregate interference distribution can be attributed only to the shadowing correlations.

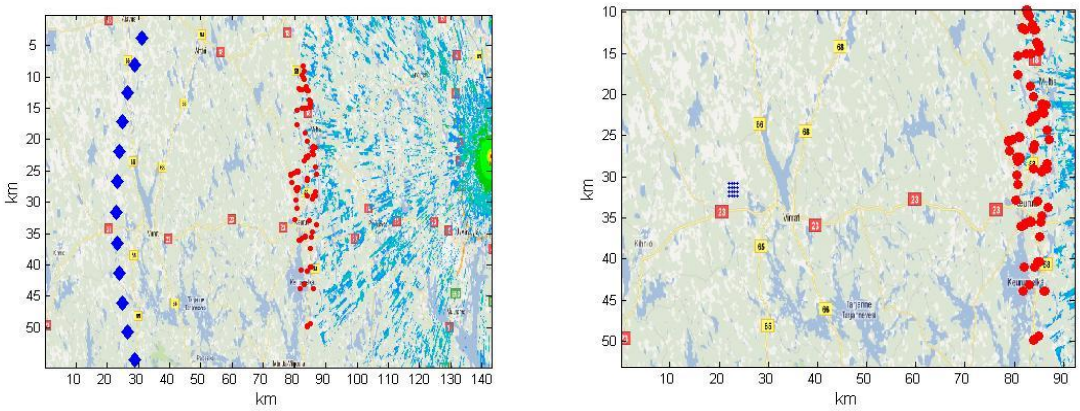

Figure 5-13: Two different deployments for the secondary users emulating correlated and independent shadowing. Independent case (left). Correlated case (right).

We compute the transmission power level for uncorrelated transmission case not violating the SIR target. By using that level we compute the SIR distribution for both cases, correlated and uncorrelated transmission (see Figure 5-14). As expected, the distribution of the aggregate interference for the correlated case is characterized by a higher variance. For the secondary deployment depicted in Figure 5-13 (left) the correlation coefficient between any pair of secondary users lies between -0.3 and 0.4. On the other hand, for the correlated case the values of the correlation coefficient are between 0.7 and 0.94.

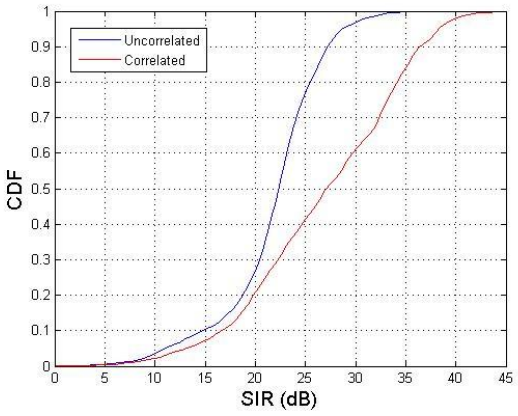

Figure 5-14: Distribution of aggregate interference for the secondary deployments depicted in Figure 5-13. The transmission power (common for all secondary transmitters) is set based on the uncorrelated case.

5.4 Comparing the model with current proposal by ECC

In Section 5.1 and 5.2 we show that the spatial power density emitted from the secondary deployment area is sufficient to describe the generated interference at the TV test points. In Section 5.3 we tested the feasibility of the power density proposal in a realistic environment by taking into account the terrain morphology. It was shown that the secondary deployment area could be split into multiple regions. The spatial power density emitted from a region is sufficient to describe the aggregate interference from secondary transmitters located inside that region. In this section we compare the spatial power density method with the current ECC approach. The target is twofold. Firstly, it is to show that the current ECC approach violates the TV protection criteria while the proposed approach does not. Secondly, it is to show that the spatial power density approach can result in higher transmission power levels and hence higher secondary throughput compared to the current ECC method.

We consider the Vihtavuori TV transmitter in Finland with operational frequency $f_{TV} = 546$ MHz. At this frequency the minimum required wanted field strength for the TV signal is 53.26 dBu. The location probability is commonly taken equal to $q = 90\,\%$. The standard deviation of the slow fading variations for the TV and the interfering signal are both taken equal to $\sigma_{TV} = \sigma_{SU} = 5$ dB. The fading margin related to the variations between the TV and the interfering signal is equal to $q \cdot \sqrt{\sigma_{TV}^2 + \sigma_{SU}^2} = 9$ dB. In order to make the results by using the two approaches comparable, the impact of noise has been ignored in the proposed approach too. The pixel size is taken equal to 250 m x 250 m. The secondary antenna is assumed to be placed outdoors at 10 m height. At the same height the TV receivers are assumed to be placed. The Okumura-Hata propagation model in suburban environment is used in our calculations. The aggregate interference will be computed at the TV test points. All the points in the TV coverage area are considered to be test points.

5.4.1 Case study: large secondary area

The secondary network is deployed near to the TV coverage area border. The secondary deployment area is assumed to be a square with side 10 km. For the selected pixel size, 1600 pixels are needed to cover the secondary area.

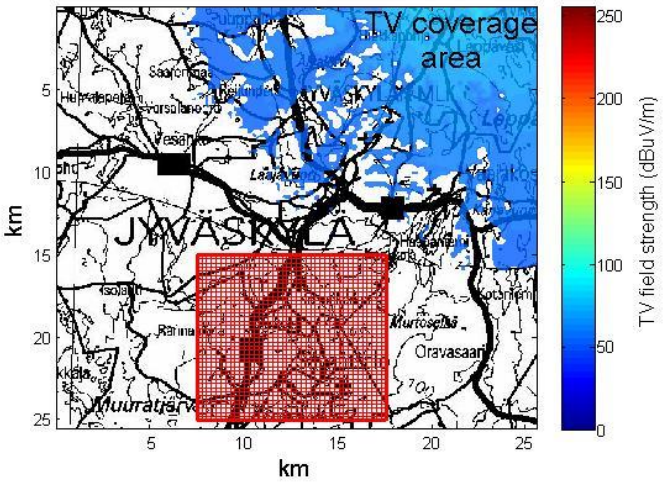

Figure 5-15: Part of the coverage area of the TV transmitter in blue and grid of secondary deployment area in red. The side of the secondary deployment area is 10 km.

In order to identify the transmission power level for each pixel of the secondary deployment area the following equation from [42] has been used:

$$P_{SU} = \sqrt{\sigma_{TV}^2 + \sigma_{SU}^2} \cdot Q^{-1}(1-O) + M_{TV} - 10\log_{10}(\Gamma_t) + PL(d) + M \qquad (5\text{-}3)$$

where $PL(d)$ is the path loss attenuation in dB as a function of the distance separation d between the WSD and the TV cell border and M incorporates the multiple interference and the safety margin.

The multiple interference margin is taken to be 6 dB. For safety margin equal to 10 dB and 19 dB the average transmission power in the secondary deployment area is equal to 21 dBm and 12 dBm respectively (see Figure 5-16).

By using the power density approach and enforcing the same power level for all pixels the transmission power level is only equal to 0.1 dBm, see Figure 5-17 (left). However, if the area is split into 64 regions the average transmission power can increase to 5.6 dBm, see Figure 5-17 (right). The interference margin is equally allocated between the different regions. As we see the approach allows allocation of different power densities to different areas. Such freedom is useful if there is a need to tailor the transmission power for particular transmission needs.

The transmission power can be further increased if some of the regions are kept inactive. The mean power equals 8.6 dBm and 11.3 dBm in Figure 5-18 (left) and Figure 5-18 (right) respectively.

In Figure 5-19 the SIR distribution at the TV test points is depicted. One can see that the power allocation obtained by ECC (see Figure 5-16) violates the SIR target for both values of the safety margin. The reason being that, the amount of transmitters is large and the utilized margins (multiple interference and safety margin) are not sufficient to guarantee the TV protection criteria are fulfilled. On the other hand, the proposed approach has built-in interference control and the SIR target is not violated at all. While computing the SIR distribution based on the ECC method, it is assumed there is an active secondary transmitter inside each pixel. For the considered pixel size, 250 x 250 m^2, this might be unlikely to occur for cellular type of secondary transmitters. For low-power transmitters placed at the ground level even many transmitters can be located inside the same pixel. One can argue due to MAC scheme the transmitters will not be active simultaneously. The existing ECC algorithm is not able to control the activity factor of secondary transmitters and guarantee the primary protection. This example is used as an illustration to show that existing ECC approach is unable to cope with aggregate interference in all cases.

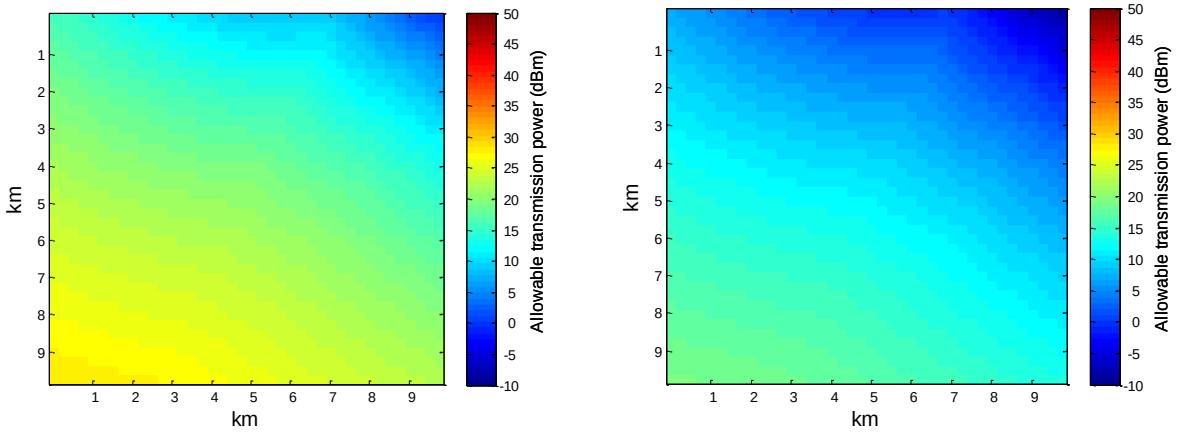

Figure 5-16: Allowable transmission power in each pixel of the secondary deployment area by using the ECC proposal. The multiple interference margin is taken equal to 6 dB. The safety margin is taken equal to 10 dB (left) and equal to 19 dB (right).

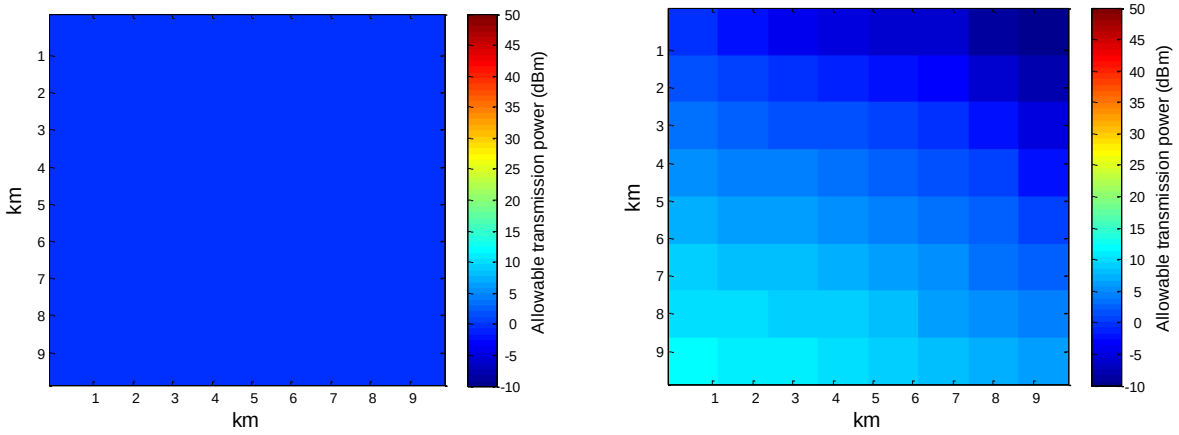

Figure 5-17: The allowable transmission power for each pixel is calculated by using the proposed approach. All secondary pixels are forced to use the same transmission power (left). The secondary pixels are grouped into square regions (right). In this example each region contains 25 pixels. The interference margin is equally allocated to all the regions. The same transmission power is used for pixels belonging to the same region.

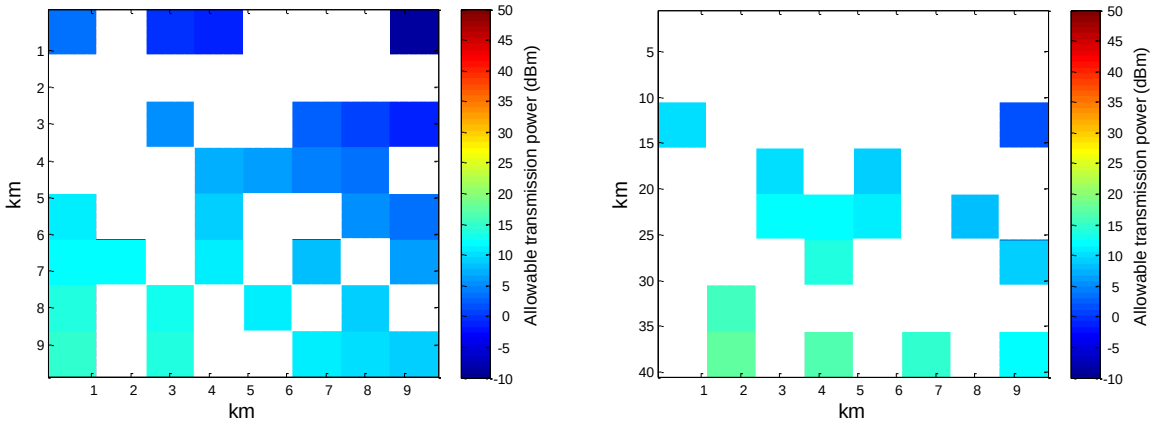

Figure 5-18: The allowable transmission power for each pixel is calculated by using the proposed approach. The secondary pixels are grouped into regions as in . Then it is assumed that only some regions are active. The active regions are randomly selected. 30 active regions (left) and 15 active regions (right) The inactive regions are marked in white. The interference margin is equally allocated to all the all active regions.

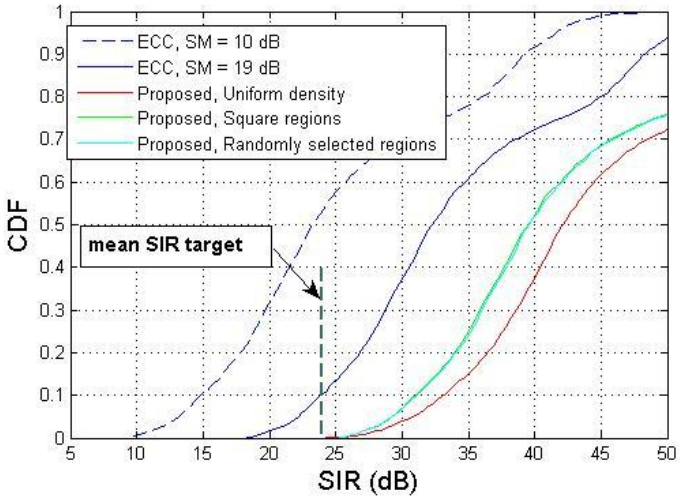

Figure 5-19: Distribution of the mean SIR over the TV test points. The target mean SIR is equal to 24 dB. The transmission power allocation by using the ECC rules results in the violation of the target SIR by using either values for the safety margin. The transmission power allocation by using the proposed approach does not violate the SIR target for any of the configurations depicted in Figure 5-17 and Figure 5-18.

Next, we illustrate that the proposed approach can allocate also higher transmission power compared to ECC proposal without violating the TV SIR target. In Figure 5-20 the secondary deployment area is split into square regions as in Figure 5-17 (right). However, in some of the regions only one pixel is active.

In Figure 5-20 (left) the allocated power to the active pixel is 2 dBm while the allocated power by using ECC rules and safety margin 19 dB is -5 dBm, Figure 5-16 (right). In Figure 5-20 (right) only one pixel in each region is active. The average power over all active pixels is equal to 20 dBm while by using the ECC proposal it is 12 dBm for safety margin 19 dB. The higher power is possible since the algorithm prohibits transmission in nearby locations. The result illustrates the flexibility of the proposed method.

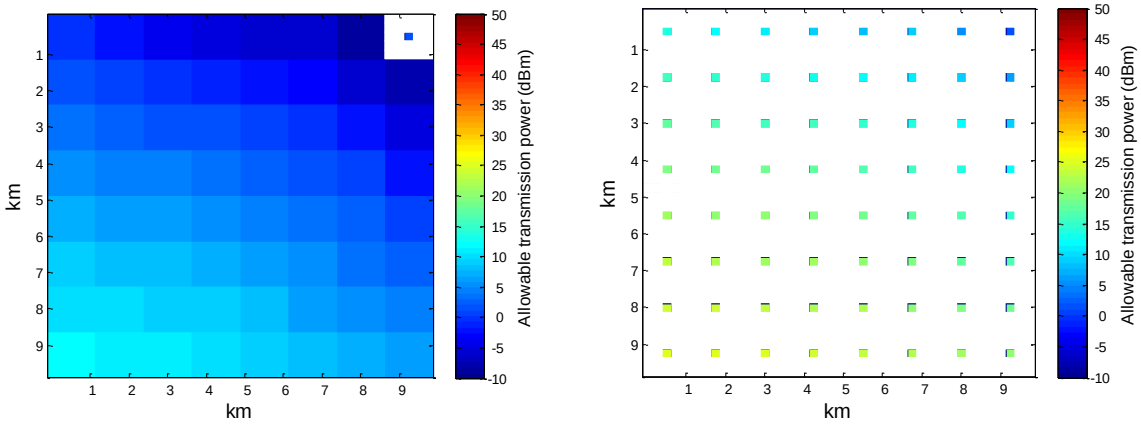

Figure 5-20: The allowable transmission power for each pixel is calculated by using the proposed approach. The interference margin is equally allocated to all the regions. The same transmission power is used for pixels belonging to the same region. Inside one of the region only a single pixel is active (left). Only a single pixel in each region is active (right).

In Figure 5-20 (right) a single secondary transmitter is active in an area equal to $1km^2$. This secondary system setup resembles cellular network with reuse distance equal to one. The existing ECC algorithm does not consider the secondary-self-interference while determining the transmission power level for each secondary pixel. The purpose of this

section is to compare the ECC method and the power density approach in terms of primary protection and secondary transmission power level allocation. Because of that, we did not consider the impact of secondary self-interference either, while determining the allocated power density to a group of secondary pixels. The impact of secondary self-interference on the allocated transmission power level will be studied in Section 5.5.

5.4.2 **Case study: small secondary area**

So far, the calculated transmission power levels for the proposed approach are in the order of 20 dBm. This power level is sufficient for a WLAN type of network but for cellular networks it is not. The transmission power levels can be further increased by deploying the secondary network far away from the TV coverage area. This is illustrated in following figure.

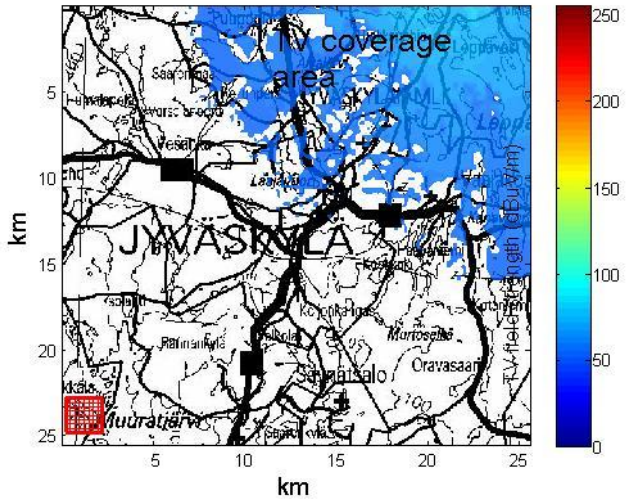

Figure 5-21: Part of the coverage area of the TV transmitter in blue and grid of secondary deployment area in red. The side of the secondary deployment area is 2 km.

The same set of figures as in Section 5.4.1 is generated. The mean transmission power levels for ECC allocation rules are equal to 30.5 dBm and 21.5 dBm for safety margin equal to 10 dB and 19 dB respectively (see Figure 5-22). When all secondary pixels are kept active the proposed approach results in 28.4 dBm mean transmission power level (see Figure 5-23). The transmission power level raises to 34.4 dBm if the deployment area is divided into 16 square regions and only one pixel per region is kept active, Figure 5-24 (left). In addition, if some regions are not active at all, the transmission power can reach up to 40 dBm, Figure 5-24(right).

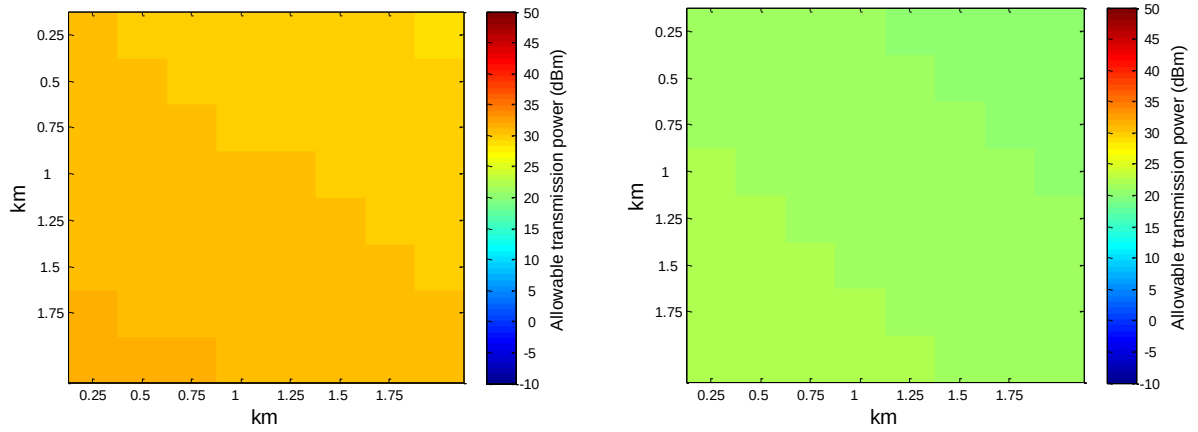

Figure 5-22: Allowable transmission power in each pixel of the secondary deployment area by using the ECC rules. The multiple interference margin is taken equal to 6 dB. The safety margin is taken equal to 10 dB (left) and equal to 19 dB (right).

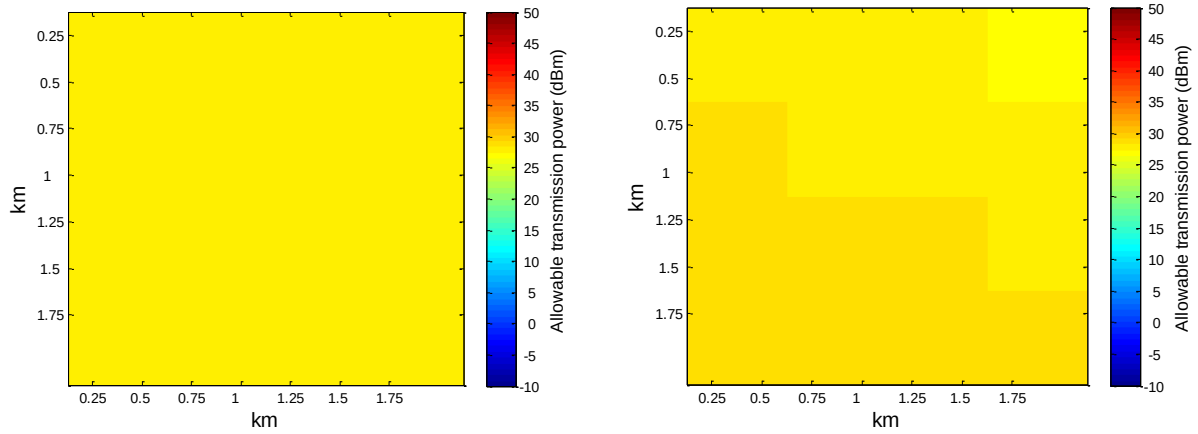

Figure 5-23: The allowable transmission power for each pixel is calculated by using the proposed approach. All secondary pixels are forced to use the same transmission power (left). The secondary pixels are grouped into square regions (right). In this example each region contains 4 pixels. The interference margin is equally allocated to all the regions. The same transmission power is used for pixels belonging to the same region.

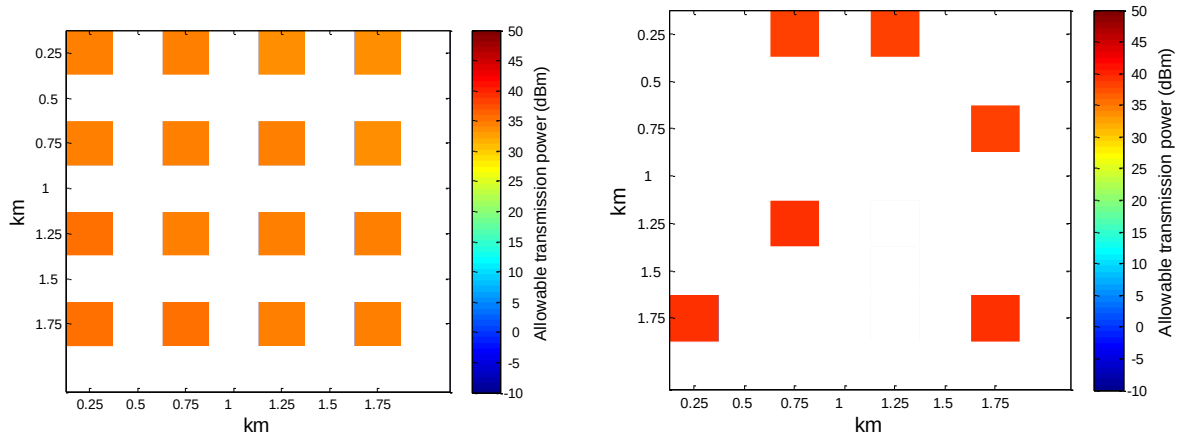

Figure 5-24: The allowable transmission power for each pixel is calculated by using the proposed approach. The interference margin is equally allocated to all the regions. Only a single pixel in each region is active. All regions are active (left). Six active regions are selected randomly (right).

The distribution of the SIR at the TV test points is depicted in Figure 5-25. By using the ECC approach the SIR target is not violated if safety margin equal to 19 dB is selected. However the transmission power in the area has been conservatively allocated. The average allocated power is only 21.5 dBm, Figure 5-22 (right). By using the proposed approach the average allocated power lies in the range 28.4 dBm to 40 dBm (see Figure 5-23 and Figure 5-24), which is considerably higher as compared to current SE43 method.

In Figure 5-24 the allocated powers are in the order of the transmission powers suggested by FCC (4W EIRP), illustrating that the proposed approach can allocate considerably higher transmission powers that was previously suggested and at the same time respects the TV SIR target (24 dB in this example). Also, in Figure 5-25 one can observe that the SIR distributions for all four examined cases by using the proposed approach overlap. The secondary network is deployed far from the TV cell border. Because of that the power density emitted from the secondary deployment area is seen to be uniform at the TV test points.

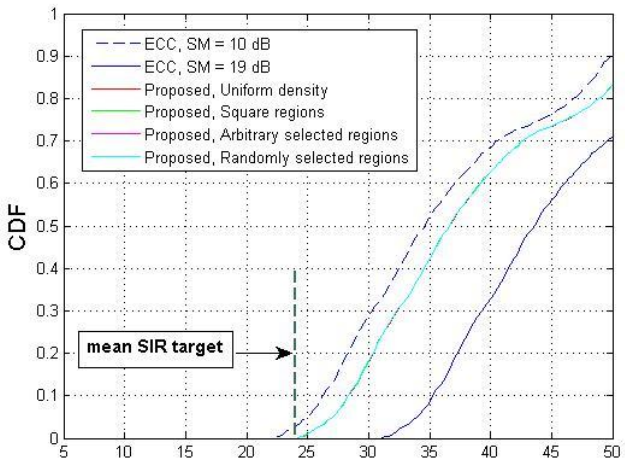

Figure 5-25: Distribution of the mean SIR over the TV test points. The target mean SIR is equal to 24 dB. The transmission power allocation by using the ECC rules results in the violation of the target SIR by using 10 dB safety margin. For safety margin equal to 19 dB the target SIR is satisfied but the allocated transmission power is low. The transmission power allocation by using the proposed

approach does not violate the SIR target for all the configurations depicted in Figure 5-23and Figure 5-24.

5.4.3 **Case study: Incorporate terrain-based channel model**

In this section we compare the spatial power density method with the current ECC proposal in a realistic environment. In Figure 5-26 the WSD are located at the corners of a 15 x 15 square grid with side equal to 2 km. Also, 1000 test points inside the TV coverage area are selected. The location probability target is $q = 90\,\%$ or equivalently, the target $\Gamma_t^{(dB)} = 15\,\text{dB}$ can be violated maximum at 100 test points.

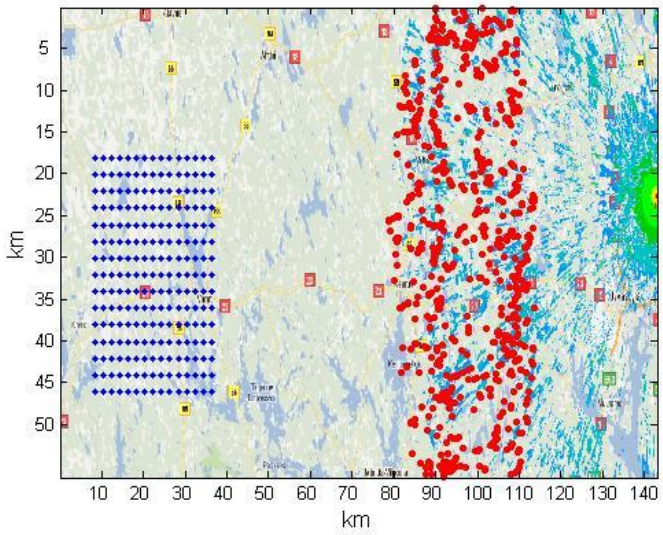

Figure 5-26: System illustration.

In Figure 5-27 the transmission power levels by using the ECC method are depicted for safety margin equal to 10 dB and 19 dB. The mean transmission power levels are equal to 16.3 dBm and 7.3 dBm respectively. One can see that due to the impact of obstruction and ground elevation, neighbouring secondary transmitters may experience significantly different path loss values to the TV test points and as such their allowable transmission power levels can differ even for 10 dB.

In Figure 5-28 (left) all secondary transmitters are forced to utilize the same transmission power level while in Figure 5-28(right) the secondary deployment area is split into 15 regions and users belonging to the same region are forced to utilize the same transmission power. The mean transmission power levels are equal to 9.9 dBm and 9.4 dBm respectively.

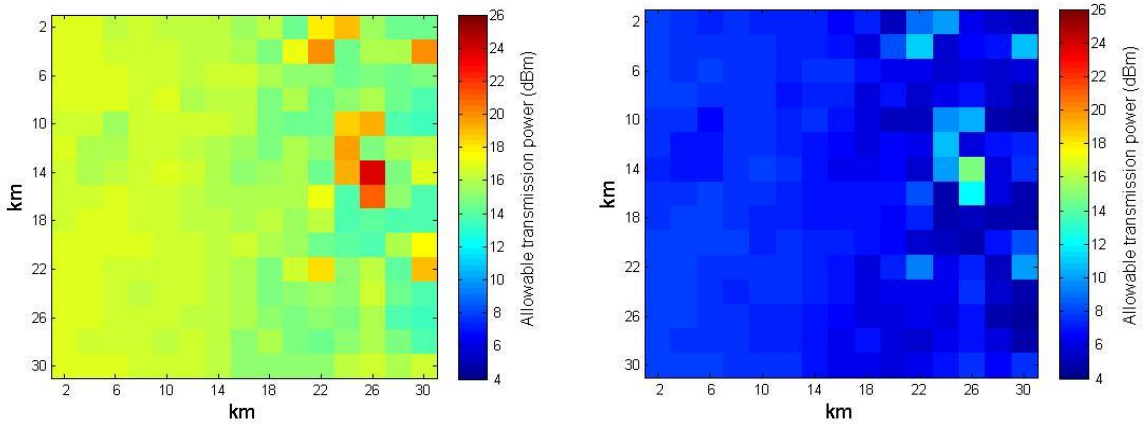

Figure 5-27: Allowable transmission power in each pixel of the secondary deployment area by using the ECC proposal. The safety margin is taken equal to 10 dB (left) and 19 dB (right). The multiple interference margin is taken equal to 6 dB.

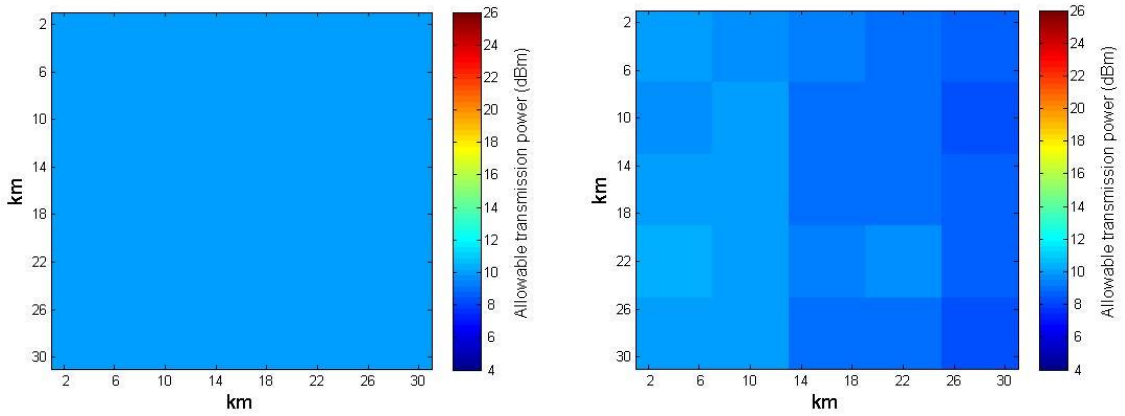

Figure 5-28: The allowable transmission power for each pixel is calculated by using the proposed approach. All secondary pixels are forced to use the same transmission power (left). The secondary pixels are grouped into square regions (right). In this example each region contains 9 pixels. The interference margin is equally allocated to all the regions. The same transmission power is used for pixels belonging to the same region.

In Figure 5-29 the secondary deployment area is split into square regions, 25 regions in Figure 5-29 (left) and 9 regions in Figure 5-29 (right) but only one pixel is active inside each region. The mean allocated power to the active pixel is 18.9 dBm and 23.4 dBm respectively. In both cases the allocated power is higher compared to the power allocated by ECC, 16.3 dBm in Figure 5-27 (right). The higher power is possible since the algorithm prohibits transmission in nearby locations.

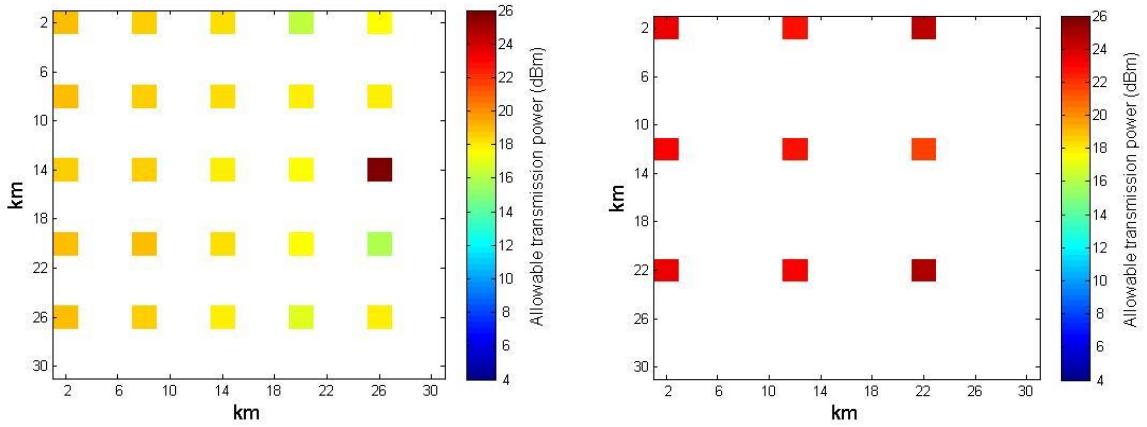

Figure 5-29: The allowable transmission power for each pixel is calculated by using the proposed approach. The secondary pixels are grouped into regions. Then it is assumed that only one pixel is active inside a region. The interference margin is equally allocated to all the all active regions. 25 regions (left) and 9 regions (right).

Finally, in Figure 5-30 the SIR distribution at the TV test points is depicted when the ECC approach and the area-based power allocation method are utilized. Due to the impact of terrain, the slow fading standard deviation for different TV test points can be different. As a result the target mean SIR for different TV test points would have been different. Because of that, unlike the results presented in Section 5.4.1 and 5.4.2, we do not convert the SIR distribution to the mean SIR distribution. One can see that for 10 dB safety margin the ECC method allocates high transmission power levels that violate the protection criteria at the TV test points. For 19 dB safety margin the TV test points are protected but the allocated transmission power levels are rather conservatively set. On the other hand, the area-based method can allocate higher transmission power levels compared to ECC without violating the SIR target at the TV test points.

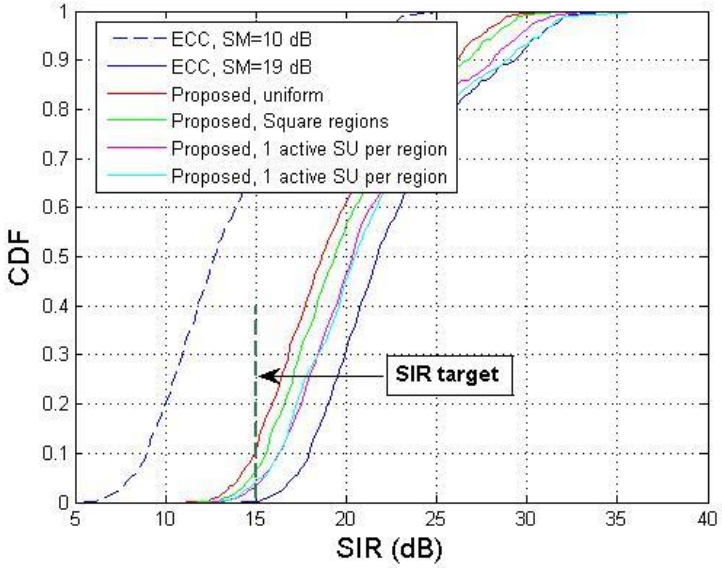

Figure 5-30: Distribution of the SIR over the TV test points. The target SIR is equal to 15 dB and the outage probability target is 10%. The transmission power allocation by using the ECC rules results in the violation of the target SIR by using 10 dB safety margin. The transmission power allocation by using the proposed approach does not violate the SIR target for all the configurations depicted in Figure 5-28 and Figure 5-29.

5.5 Incorporating secondary self-interference

In Section 5.4 we show how to set the transmission power level for a set of secondary transmitters without violating the protection criteria of TV receivers. The transmitters were grouped into multiple regions. Different regions were allocated an equal amount of the available interference margin at the TV test points. It was noticed that regions deployed far from the TV cell border are associated with high power density values at the cost of regions located close to the TV coverage border which will remain practically silent. Inside each region the secondary transmitters are allocated the same transmission power level and subsequently the allocated interference margin is split unequally among them.

In this section we propose an alternate way of splitting the available interference margin between the secondary transmitters. For illustration purposes we consider a cellular secondary network deployed in the TVWS. We set the transmission power levels to the secondary base stations so that the sum cell border capacity of the secondary network is maximized and the TV protection criteria are satisfied. At the same time, a minimum data rate requirement at the cellular cell border has to be maintained. Due to the additional cellular constraint, the interference margin is not split equally between the secondary transmitters. Secondary cells located close to the TV cell border take most of the available margin in order to satisfy their own data rate constraints. Only a small bite out of the available margin is left for the secondary cells located far from the TV cell border. However, these cells are also associated with a high path loss to the TV test points. In this set up it is noticed that the optimal transmission power levels become approximately uniform over the secondary deployment area.

The Federal Communication Committee (FCC) in US proposed a fixed transmission power level rule for all secondary transmitters with a protection area around the TV coverage border [43]. However, the common transmission power level should not be arbitrarily set equal to $4\,\mathrm{W}$ as proposed by FCC [48] but according to the interference margin available at the borders of the TV and secondary cells. When the secondary cell size can vary based on the population density the optimal transmission power levels result in approximately uniform spatial power density emitted from the secondary deployment area [56]. The illustrations presented in this section are useful for determining country-wide power allocation for cellular networks in the TVWS.

5.5.1 Problem formulation

While planning a cellular network a target data rate has to be guaranteed at the cellular end users. In order to offer the target data rate at the cellular cell border a target SINR γ_t has to be satisfied with specific outage probability O_{SU} due to the slow fading. The impact of fast fading on the achievable data rate is ignored which is a valid assumption for a low mobility scenario.

By following a similar approach as in [47] for computing the interference margin at the TV cell border, one can compute the interference margin at the cellular cell border

$$I_{\Delta,i}^{(SU)} = \exp\left(\frac{M_{I,i}}{\xi} + \frac{\sigma_{I,i}^2}{2\xi^2}\right) - \exp\left(\frac{\sigma_{TV}^2}{2\xi^2}\right) \cdot \sum_m P_m A_{TV}\left(r_{m,i}\right) - p_N \qquad (5\text{-}4)$$

where the index i is used to indicate the test point at the border of the secondary cell where the available margin is computed, $M_{I,i} = Q^{-1}\left(1-O_{SU}\right)\sqrt{\sigma_{SU}^2 + \sigma_{I,i}^2} - \xi \ln\left(\gamma_t\right) + m_{SU,i}$, σ_{SU} is the standard deviation of the useful secondary signal, $\sigma_{I,i}$ is the standard deviation of the interfering signal, $m_{SU,i}$ is the useful signal at the ith test point and p_N is the noise power level at the secondary receivers.

The interference margin (5-4) at the cellular cell border depends on the locations of the interfering TV transmitters and other cellular base stations through the parameter $\sigma_{I,i}$. Because of that, the derivation of the transmission power level for each secondary base station will be computationally expensive. Unlike the TV test points where the generated interference is much smaller compared to the useful TV signal level, the generated interference at the cellular test points is comparable to the useful signal level. Because of that the approximation introduced by setting $\sigma_{I,i}=0$ in (5-4) may not be tight.

For the system setup illustrated in Figure 5-1 we identify the common maximum allowable transmission power level for the cellular base stations such that the interference margin at the TV and the cellular test points is not violated. For the TV test points the interference margin given in equation (5-1) is used. For the cellular test points we use the interference margin (5-4) and also the value of margin by setting $\sigma_{I,i}=0$. In Figure 5-31 the calculated power density is depicted for different secondary cell radiuses. One can see that by setting $\sigma_{I,i}=0$ we derive a lower bound on the allowable transmission power. The lower bound is tight unless the standard deviation of the slow fading becomes high.

Hereafter, the lower bound on the interference margin at the cellular test points is used by setting $\sigma_{I,i}=0$ in (5-4):

$$I_{\Delta,i}^{(SU)}=\exp\left(\frac{M_{I,i}}{\xi}\right)-\exp\left(\frac{\sigma_{TV}^2}{2\xi^2}\right)\sum_m P_m A_{TV}\left(r_{m,i}\right)-P_n \qquad (5\text{-}5)$$

where $M_{I,i}=Q^{-1}\left(1-O_{SU}\right)\cdot\sigma_{SU}-\xi\ln\left(\gamma_t\right)+m_{SU,i}$.

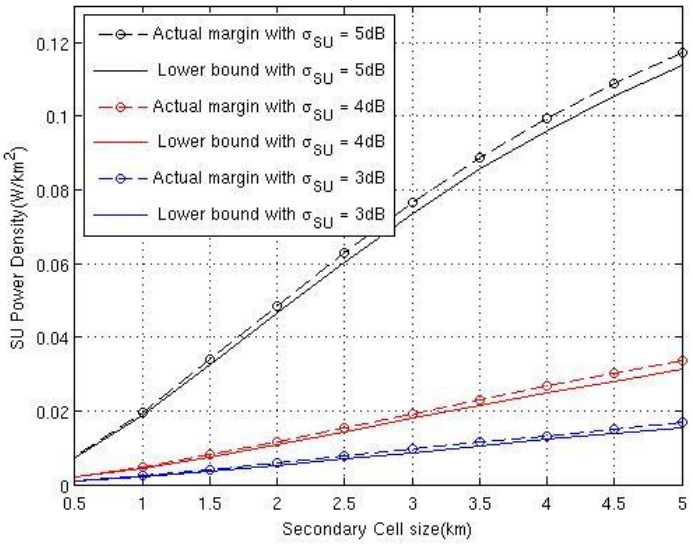

Figure 5-31: Maximum allowable Spatial power density emitted from the secondary deployment area such that the TV and cellular interference margin is not violated.

We want to set the transmission power levels at the cellular base stations such that the sum cell border capacity is maximized and the interference margin is not violated both at the cellular and the TV test points. Mathematically, the problem can be formulated as:

$$\begin{aligned} \underset{\mathbf{p}}{\text{Maximize}}: \quad & \sum_i \log_2\left(1+\overline{\gamma}_i\right) \\ \text{Subject to}: \quad & \sum_k p_k A_{SU}\left(r_{k,j}\right) \le \exp\left(-\frac{\sigma_{SU}^2}{2\xi^2}\right)\cdot I_{\Delta,j}^{(TV)}, \forall j \\ & \sum_{k\neq k'} p_k A_{SU}\left(r_{k,i}\right) \le \exp\left(-\frac{\sigma_{SU}^2}{2\xi^2}\right)\cdot I_{\Delta,i}^{(SU)}, \forall i \end{aligned} \tag{5-6}$$

where $\overline{\gamma}_i$ is the average SINR at the i th cellular test point:

$$\overline{\gamma}_i = \frac{p_{k'} A_{SU}\left(r_{k',i}\right)}{\sum_{k\neq k'} p_k A_{SU}\left(r_{k,i}\right) + \sum_m P_m A_{TV}\left(r_{m,i}\right) + P_n} \tag{5-7}$$

The optimization problem (5-6) is a non-convex problem and it is solved numerically by using the numerical optimization toolbox in MATLAB.

5.5.2 **Numerical illustrations**

The system model is same as the one described in Section 5-1 and the parameter settings for the cellular and the TV system were summarized in Table 5-1 and Table 5-2 respectively. Additionally, we assume that the outage probability target at the cellular cell borders is $O_{SU} = 10\%$ for SINR target equal to $\gamma_t = -3.5$ dB. The cellular test points are taken to be the vertices of the hexagonal-shaped cells. The cellular cell radius is taken equal to 1 km. Also, the reuse distance for the cellular network is set equal to 3. For reuse distance equal to 1 it is not possible to satisfy the cellular protection constraints even in the absence of TV interference. In the solution of the optimization problem (5-6) the maximum transmission power level is taken equal to 100 W.

Firstly, we compute the power allocation at the cellular base stations without considering the cellular coverage constraints. When the cellular constraint is not taken into account, see Figure 5-32, the cells located close to the TV cell border utilize very low transmission power level in order not to violate the TV interference margin. The power level for the cellular base stations increases gradually as we move further from the TV cell border. As a result the distribution of transmission power level over the secondary deployment area is not uniform. Since the optimization objective is the sum capacity maximization the cells that are located close to the TV cell border sacrifice their capacity for the sake of the cells that are located far from the TV cell border.

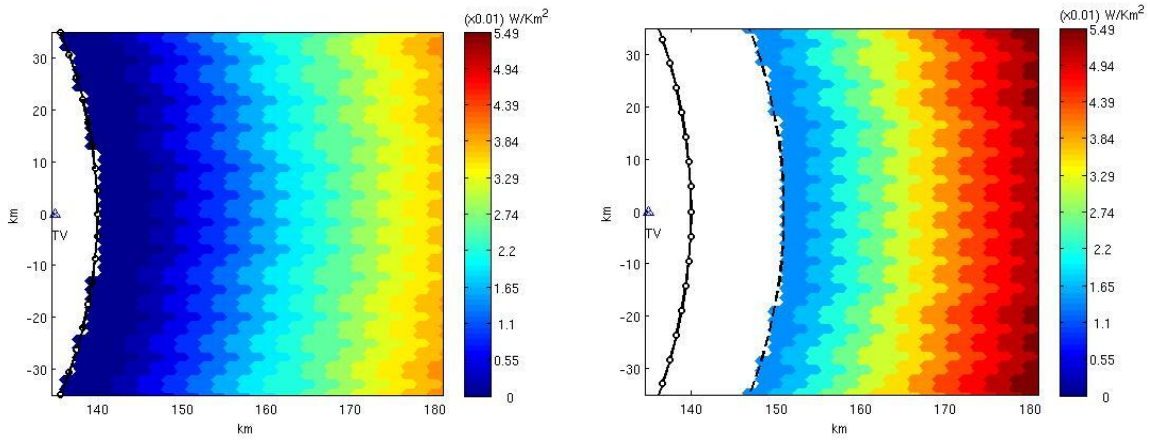

Figure 5-32: Spatial power density emitted from the secondary deployment area. The transmission power levels for the cellular base stations are calculated by solving optimization problem (5-6) without cellular constraints.

If a minimum data rate requirement has to be satisfied also for the cellular network the trend in transmission power level allocation becomes completely different. Few observations can be made based on Figure 5-33. Firstly, some protection distance is required in order to obtain feasible solutions in the optimization problem (5-6). Secondly, the cells that are located close to the TV cell should utilize enough transmission power to satisfy their own coverage constraint. Because of that only a small portion of the interference margin is left for cells located further away. This justifies the approximately uniform transmission power allocation level demonstrated in Figure 5-33. One may argue that the approximately same transmission power level is due to the protection distance. However, it is the cellular coverage constraints that prohibit cells located far from the TV cell border to utilize high transmission power levels, compare Figure 5-33 and Figure 5-32 (right).

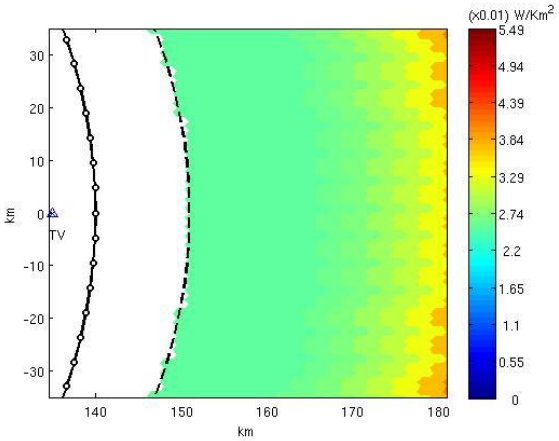

Figure 5-33: Spatial power density emitted from the secondary deployment area. The transmission power levels for the cellular base stations are calculated by solving optimization problem (5-6) with cellular constraints.

This observation motivates us to identify the common transmission power level for cellular base stations that satisfies both TV and cellular coverage constraints. Mathematically, the optimization problem can be formulated as:

$$\begin{aligned} \underset{p_{SU}}{\text{Maximize}}: \quad & \sum_i \log_2\left(1+\overline{\gamma}_i\right) \\ \text{Subject to}: \quad & p_{SU} \le \exp\left(-\frac{\sigma_{SU}^2}{2\xi^2}\right)\cdot\frac{I_{\Delta,j}^{(TV)}}{\sum_k A_{SU}\left(r_{k,j}\right)}, \forall j \\ & p_{SU} \le \exp\left(-\frac{\sigma_{SU}^2}{2\xi^2}\right)\cdot\frac{I_{\Delta,i}^{(SU)}}{\sum_{k\neq k'} A_{SU}\left(r_{k,i}\right)}, \forall i \end{aligned} \tag{5-8}$$

This is a convex optimization problem because the optimization constraints are linear and the optimization objective is a sum of increasing convex functions [55]. The optimization problem (5-8) can be solved by using standard interior point methods. The optimal solution for the secondary deployment area depicted in Figure 5-33 is equal to 0.2 W. The corresponding power density value is equal to 0.026 W/km^2 which is close to the one depicted in Figure 5-33.

The accuracy of the constant transmission power level approximation for different cell sizes and protection distances is illustrated in Figure 5-34. One can observe that the capacity calculated by optimizing the transmission power of individual base stations is only slightly more compared to the capacity obtain for uniform transmission power allocation. The approximation accuracy improves for larger protection distances. When the cellular network is deployed far from the TV cell border, the impact of TV

interference becomes marginal. The cellular system can essentially reach interference limited mode and all base stations utilize the maximum allowable transmission power.

Note also that for 2 km cell radius the optimization problems (5-6) and (5-8) do not give any feasible solution for protection distance equal to 11 km. The cellular base stations deployed close to the TV cell border cannot utilize high enough transmission power for meeting their own coverage constraints without violating the TV constraints.

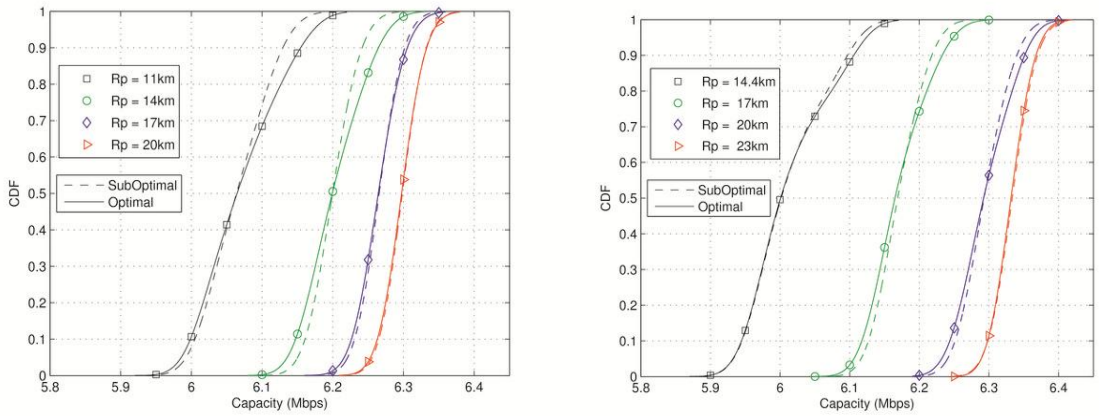

Figure 5-34: Distribution of cell border capacity by optimizing the transmission power level for each base station individually, optimization problem (5-6), and by using the uniform power allocation approximation, optimization problem (5-8). The cell radius is equal to 1 km (left) and 2 km (right).

Next we show that the uniform power allocation approximation can be used to plan a cellular secondary TVWS network in a country-wide level. Unlike the above described case, the cell size over a country should not be kept constant but should vary according to the population density. The population density and a potential cellular layout for Finland are depicted in Figure 5-35. Three different cell types for urban, suburban and rural environment are used with cell radius equal to 0.5 km, 2km and 5 km respectively. At a particular location the cell type is selected such that the population density in a cell does not exceed the 10 000 inhabitants per km^2.

We consider setting the transmission power level at TV channel 22. Following the FCC rules the secondary transmitters falling inside the protection area of the co-channel and the first adjacent channels remain silent, TV black space.

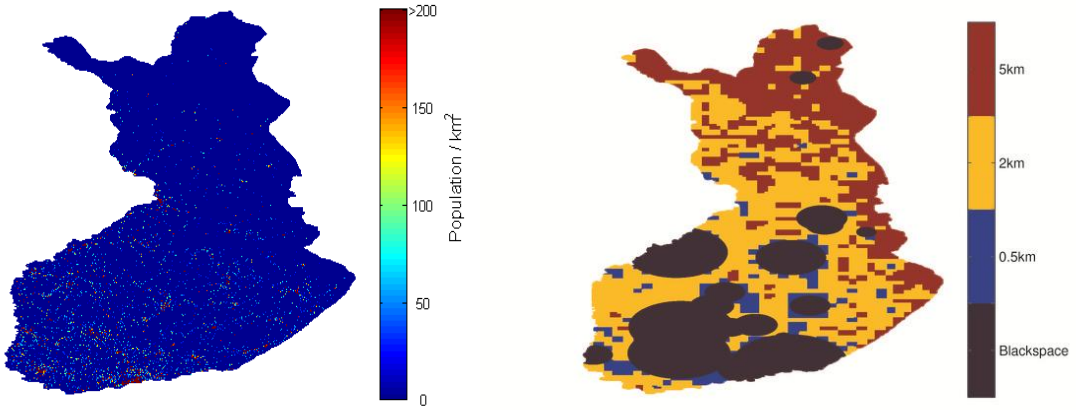

Figure 5-35: Population density in Finland (left). Cellular layout based on user density (right). The TV black space is the protection area of the TV transmitters operating in channel 22 and also of the TV transmitters operating in the two first adjacent channels. The protection distance for the co-channel is taken equal to 14.4 km and for the adjacent channels equal to 0.74 km.

Initially, it is assumed that the cells of the same type utilize the same transmission power level. The transmission power levels by solving the optimization problem (5-6) are equal to 44 mW, 770 mW and 5.1 W for urban, suburban and rural cells respectively. The corresponding power density values are equal to 44 mW/km^2, 48mW/km^2 and 51mW/km^2. One can deduce that the spatial power density emitted all over the country appears to be constant. If the optimization problem (5-6) is solved by enforcing constant power density, the optimal value is equal to 49 mW/km^2 and the transmission power levels for urban, suburban and rural cells equal to 49 mW, 780 mW and 4.9 W. The loss in the sum capacity by assuming constant power density all over the country is marginal compared to the case where the transmission power level is optimized for cells of the same type.

For illustration purposes, we use the uniform power density approximation to compute the average available capacity for a user in the TVWS at channel 22. By using the derived transmission power levels the average capacity within each secondary cell is computed and divided by the number of users populating that cell. The color-coded map of capacity per inhabitant is depicted in Figure 5-36 (left). One can see that the capacity per user becomes highest in the rural areas due to the extremely sparse population density. On the other hand, in urban and suburban areas the capacity per user is about the same. The reason being, that the higher capacity per area in urban cells is shared over a larger number of users as well. Finally, in Figure 5-36 (right) the SINR distribution at the TV and the cellular test points is depicted. The SINR targets -3.5 dB for cellular and 17 dB for TV with specified outage probability 10% are satisfied.

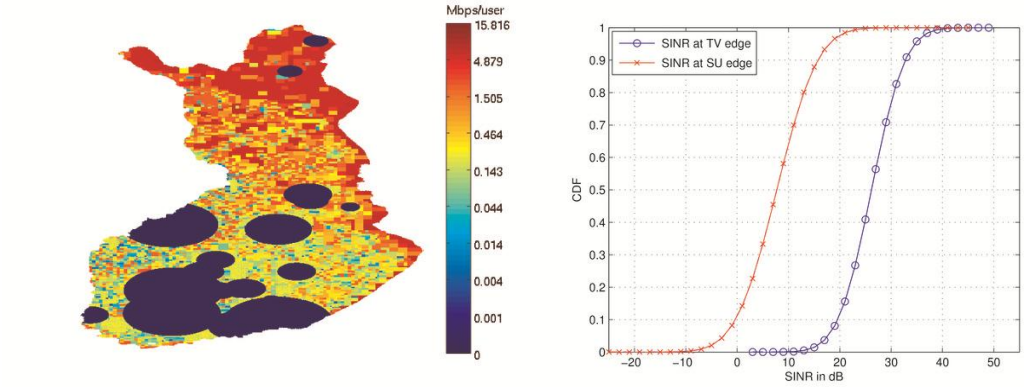

Figure 5-36: Average available capacity per user (left) Distribution of the SINR at the TV test points and the cellular test points (right). The outage probability target is 10% for SINR target equal to 17 dB for TV and -3.5 for cellular

5.6 Incorporating heterogeneous secondary user densities

In Section 5.3 we proposed a method for clustering the secondary pixels while taking into account the impact of terrain on the signal propagation. Each cluster was characterized by the following property: the spatial power density emitted from the cluster's area was sufficient to describe the aggregate interference at the TV test points. The study carried out in Section 5.3 considered only the morphology of the terrain and did not take into account the impact of non-uniform population density.

In this section we take into consideration the user density and identify how many clusters we need to generate in order to approximate close enough the distribution of the aggregate interference. We do not propose a particular clustering algorithm. We generate the clusters simply by dividing the secondary deployment area into equally-sized rectangular areas. Inside each area/cluster we utilize a PPP model for computing the aggregate interference at the TV test points. The total interference is described as a sum of the interferences from the multiple areas.

Modifying the PPP model to account for non-uniform user density has been already proposed in [54]. A PPP model assumes that the user density is uniform. Because of that it turns out that a single area does not estimate accurately enough the exact interference level at the TV test points. However, only few areas are sufficient to model the impact of non-uniform user density and approximate close enough the aggregate interference distribution.

In addition a PPP model usually assumes a simple power law based model for the signal propagation: $g(r) = c \cdot r^{-\alpha}$ and slow fading. For each area we identify the model parameters c, α, σ by fitting it into the path loss values calculated from the terrain-based model. It turns out that a power law model can be accurate enough provided its parameters are carefully selected.

5.6.1 **System model**

We consider a single TV transmitter outside Helsinki, Finland and we allocate inside its coverage area M test pixels. Each pixel is surrounded by a dense grid of L test points for modelling the impact of slow fading, Figure 5-37 (left). The distribution of the aggregate interference due to the secondary transmissions will be expressed as the histogram of the aggregate interference values in $M \times L$ TV test points.

Outside the TV protection area a WLAN type of secondary network is deployed and operates co-channel to the TV transmitter. The secondary deployment area is covered by square pixels. The amount of households inside each secondary pixel is depicted in Figure 5-37 (right). It is assumed that each household has one WLAN transmitter.

The aggregate interference at the test point m_ℓ that is the ℓ th test point around the m th test pixel is:

$$I_{m_\ell} = \nu \cdot P_{SU} \cdot \sum_n K_n \cdot g_{nm_\ell} \qquad (5\text{-}9)$$

where ν is the activity factor of the WLAN transmitters, K_n is the total number of transmitters in the n th secondary pixel and g_{nm_ℓ} is the path loss between the considered secondary pixel and the TV test point. The path loss g_{nm_ℓ} will be computed by using the terrain information [46] in splat! software package [45].

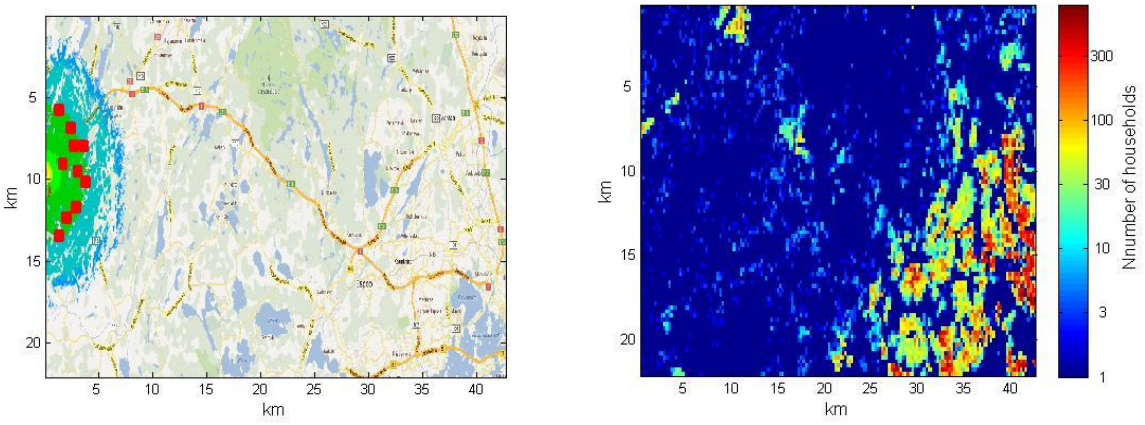

Figure 5-37: System illustration. TV coverage area, TV test points and secondary deployment area (left) and density of the households (right).

In order to approximate the distribution of the aggregate interference by using a PPP model we split the secondary deployment area S into multiple areas S_t. Inside each area the household density is assumed to be uniform. Therefore the moments of the

aggregate interference attributed to each area can be computed based on (3-24). The total interference can be described as a sum of the interference over all the areas.

From (3-25) the mean of the aggregate interference can be read as:

$$\mathrm{E}\{I_{SU}\} = \sum_t P_{d_t} \cdot \exp\left(\frac{\sigma_t^2}{2\xi^2}\right) \cdot \iint_{S_t} g(r) ds$$

where σ_t is the slow fading standard deviation and $g(r) = c_t \cdot r^{-\alpha_t}$ is the power law path loss for secondary transmissions originated from the area S_t. If the power density is written in terms of the transmission power P_{SU} and the average footprint A_f we get:

$$\mathrm{E}\{I_{SU}\} = \sum_t \frac{N_t}{S_t} \cdot P_{SU} \cdot \exp\left(\frac{\sigma_t^2}{2\xi^2}\right) \cdot \iint_{S_t} g(r) ds \qquad (5\text{-}10)$$

where $A_f = S_t / N_t$ and N_t is the average number of active transmitters in the area S_t.

Similarly, by using (3-26) we can write the second moment of the aggregate interference as:

$$\mathrm{E}\{I_{SU}^2\} = \sum_t \frac{N_t}{S_t} \cdot P_{SU}^2 \exp\left(\frac{2\sigma_t^2}{\xi^2}\right) \cdot \iint_{S_t} g^2(r) ds + \mathrm{E}^2\{I_{SU}\} \qquad (5\text{-}11)$$

Note that the first term of (5-11) is the variance of the aggregate interference and the second term is the square of the mean given in (5-10).

5.6.2 **Channel model parameterization**

It is assumed that all transmissions inside an area be described by the same power law based model, $c_t \cdot r^{-\alpha_t} \cdot 10^{X_t/10}$. The parameters α_t, c_t, σ_t will be different for different TV test points. In order to parameterize the channel model, we compute the first two moments of the aggregate interference from an area S_t by using the power law and the terrain-based model. The mean of the aggregate interference from the area S_t by using the power law model and after expressing the integral as a sum is:

$$\mathrm{E}\{I_{SU}\} = \frac{N_t}{S_t} \cdot P_{SU} \cdot c_t \cdot e^{\frac{\sigma_t^2}{2\xi^2}} \cdot S_p \cdot \sum_{n \in S} r_{nm}^{-\alpha_t} \qquad (5\text{-}12)$$

where r_{nm} is the distance between the nth secondary pixel and the mth TV test pixel and S_p is the area of a secondary pixel. Note that the term $N_t S_p / S_t$ describes the average number of active transmitters per pixel in the area S_t.

Similarly, by using the terrain-based channel model the mean aggregate interference is:

$$\mathrm{E}\{I_{SU}\} = \frac{N_t \cdot S_p}{S_t} \cdot P_{SU} \cdot \frac{1}{L} \cdot \sum_{n \in S_t} \sum_{\ell} g_{nm_\ell} \qquad (5\text{-}13)$$

By enforcing the right-hand side of (5-12) and (5-13) to be equal we get:

$$c_t \cdot e^{\frac{\sigma_t^2}{2\xi^2}} \cdot \sum_{n \in A_t} r_{nm}^{-\alpha_t} = \frac{1}{L} \sum_{n \in S_t} \sum_{\ell} g_{nm_\ell} \qquad (5\text{-}14)$$

Similarly, one can compute the second moment of the aggregate interference from an area S_t by using the power law and the terrain-based model. For the power law model:

$$\mathrm{E}\left\{I_{SU}^2\right\}=\frac{N_t}{S_t}\cdot P_{SU}^2\cdot c_t^2\cdot e^{\frac{2\sigma_t^2}{\xi^2}}\cdot S_p\cdot\sum_{n\in S} r_{nm}^{-2\alpha_t} \tag{5-15}$$

For the terrain-based model we compute the cross correlation between all pairs n_1, n_2 of secondary pixels inside the area S_t.

$$\mathrm{E}\left\{I_{SU}^2\right\}=\frac{N_t\cdot S_p}{S_t}\cdot P_{SU}^2\cdot\frac{1}{L^2}\sum_{n_1\in S_t}\sum_{n_2\in S_t}\sum_{\ell} g_{n_1 m_\ell}\sum_{\ell} g_{n_2 m_\ell} \tag{5-16}$$

By enforcing the right-hand side of (5-15) and (5-16) to be equal we get:

$$c_t^2\cdot e^{\frac{2\sigma_t^2}{\xi^2}}\cdot\sum_{n\in S} r_{nm}^{-2\alpha_t}=\frac{1}{L^2}\sum_{n_1\in S_t}\sum_{n_2\in S_t}\sum_{\ell} g_{n_1 m_\ell}\sum_{\ell} g_{n_2 m_\ell} \tag{5-17}$$

where n_1, n_2 are pixels in the secondary deployment area.

We have ended up with a nonlinear system of two equations, (5-14) and (5-17), with three unknowns, α_t, c_t, σ_t. One possible way to solve it is to assign some arbitrary value for the path loss attenuation exponent α_t and find c_t, σ_t satisfying (5-14) and (5-17). By taking the square of (5-14) and dividing by sides with (5-17) we can solve for the variance σ_t^2.

$$\sigma_t^2=\xi^2\cdot\ln\left(\frac{\left(\sum_{n\in S_t} r_{nm}^{-\alpha_t}\right)^2\cdot\sum_{n_1\in S_t}\sum_{n_2\in S_t}\sum_{\ell} g_{n_1 m_\ell}\sum_{\ell} g_{n_2 m_\ell}}{\sum_{n\in S_t} r_{nm}^{-2\alpha_t}\cdot\left(\sum_{n\in S_t}\sum_{\ell} g_{nm_\ell}\right)^2}\right) \tag{5-18}$$

The attenuation constant c_t for the secondary transmissions generated inside S_t can be derived from (5-14).

$$c_t=e^{-\frac{\sigma_t^2}{2\xi^2}}\cdot\frac{1}{L}\cdot\frac{\sum_{n\in S_t}\sum_{\ell} g_{nm_\ell}}{\sum_{n\in S_t} r_{nm}^{-\alpha_t}} \tag{5-19}$$

The σ_t in (5-19) has been computed in (5-18). Note that the parameters σ_t, c_t will be computed for each secondary area S_t.

If the parameters c_t, σ_t have to be computed for each secondary pixel and not for a group of secondary pixels then, (5-18) and (5-19) are degenerated to (5-20) and (5-21) respectively:

$$\sigma_t^2=\xi^2\cdot\ln\left(L\cdot\sum_{\ell} g_{nm_\ell}^2\cdot\left(\sum_{\ell} g_{nm_\ell}\right)^{-2}\right) \tag{5-20}$$

$$c_t=e^{-\frac{\sigma_t^2}{2\xi^2}}\cdot r_{nm}^{\alpha_t}\cdot\frac{1}{L}\sum_{\ell} g_{nm_\ell} \tag{5-21}$$

5.6.3 **Numerical illustrations**

We compare the exact distribution of the aggregate interference with the PPP based approximation. It is illustrated that for relatively few areas S_t the exact distribution can be described sufficiently well by using the PPP model inside each area.

In order to obtain the exact distribution of the aggregate interference we evaluate (5-9) for all TV test points. In order to approximate the distribution of the aggregate interference we first split the secondary deployment area into a certain number of areas. The mean and the variance of the total interference are computed as the sums of the means and variances of the interference from each area, (5-10) and (5-11) respectively. The mean and variance of the interference from an area are computed based on (5-12) and (5-15) respectively. The parameters σ_t, c_t in (5-12) and (5-15) are computed based on (5-18) and (5-19) respectively while the value of the path loss attenuation exponent is fixed to $\alpha_t = 4.5$ for all areas. The rest of the parameter settings for the TV and the secondary system are summarized in Table 5-3 and Table 5-4 respectively.

Table 5-3: Parameter settings for the TV system

TV system	
Test pixels	$M = 10$ test pixels and $L = 100$ test points around each pixel
Protection distance	400 m
Coverage area	A test pixel belongs to the TV coverage area if it experiences useful TV signal field strength 55.3 dBu with location probability higher than 90%

Table 5-4: Parameter settings for the secondary system

WLAN system	
Deployment area	Rectangular of size $22 \times 42\,\text{km}^2$
Pixels	The secondary deployment area is covered with square cells of size $250 \times 250\,\text{m}^2$. In terms of secondary pixels the secondary deployment area has size equal to 89×154.
Transmission powers	$P_{SU} = 10$ mW for all WLAN transmitters.
Activity factor	5 %
Path loss model	For the exact distribution of the aggregate interference the Longley-Rice model in SPLAT! software package [splat] is used along with terrain elevation data [FinnTerrain]. For the PPP model the path loss attenuation exponent is always taken equal to $\alpha_t = 4.5$. The slow fading standard deviation and the path loss attenuation constant are derived from (5-18) and (5-19)

In the extreme case where the PPP model is applied over the complete secondary area, the aggregate interference level is overestimated. In our system setup most of the households are located far from the TV cell border while, the PPP model allocates them uniformly inside the secondary area. As a result, one can see that the mean interference level is overestimated by approximately 6 dB. However, already for 64 areas the exact distribution of the aggregate interference is well approximated. Particularly in the upper tail, the exact and the approximating distributions come very close to each other.

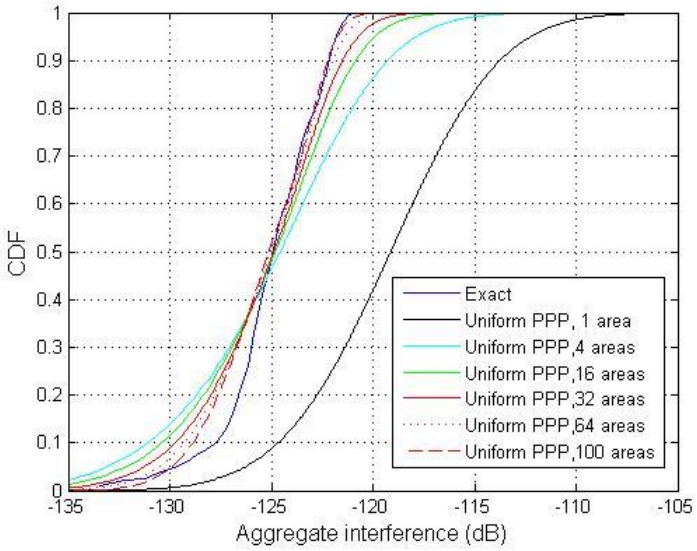

Figure 5-38: Distribution of the aggregate interference at the TV test points

The upper tail of the interference distribution is associated with the lower tail of the SINR distribution. Good match at the upper tail means that the proposed model describes well whether the SINR target at the TV receivers will be violated due to the secondary transmissions or not. One can see that the approximation error becomes negligible in the upper tail of the aggregate interference distribution as soon as the number of areas raises above 64 (see Figure 5-38). In fact, the proposed method overestimates slightly the interference level in the upper tail. Taking into consideration that the total area size is approximately 1000 km^2 the required number of areas for approximating the aggregate interference is relatively small.

6 Conclusions

In this deliverable we reviewed the current state of the art in aggregate interference modelling and proposed two new models for estimating the aggregate interference in a primary-secondary system setup. These models will serve as inputs to QUASAR WP5 for assessing the amount of available spectrum in different spectrum sharing scenarios.

The exclusion region model has been applied in the aeronautical and the meteorological radar spectrum while the power density model has been applied in the TV spectrum.

The exclusion model considers a situation where a primary receiver is interfered by many secondary transmitters spreading in a large area. This model well describes the secondary access to radar or aeronautical spectrum where primary receivers of high interference susceptibility are sparsely located. The protection of the primary receiver is achieved by each secondary user's decision based on the estimation of propagation loss. Through mathematical analysis, the cumulants of aggregate interference are derived. Then, the PDF of aggregate interference is approximated with the method of moments.

The exclusion region model is first illustrated with the assumption of homogeneous (uniform) secondary user density and the perfect estimation of the propagation loss. The model can be extended to several directions: The exclusion region model can incorporate the effect of heterogeneity in the spatial distribution of the secondary users. We introduced the concept of hot zone, which is an annulus sector with higher secondary user density overlaid on the background circle. Based on our results for the hot zone model, it is shown that heterogeneous density of secondary users has significant impact on the aggregate interference only when the hot zone is close to the primary victim. Otherwise, heterogeneity on the spatial distribution does not need to be considered.

In addition, we elaborated on the characteristics of radar that an antenna of sharp beam width rotates in a regular and predictable manner. Secondary users can exploit temporal opportunities in the radar spectrum when they have exact information about the real-time radar activity. This could significantly increase the opportunities of the secondary users. However, having precise knowledge about the rotation pattern of the radar is still a technical challenge. Finally, we investigated the impact of uncertainty in the propagation loss for the application of our model to aeronautical spectrum. When we consider distance measurement equipment (DME) as a potential primary victim, secondary users have uncertainty in the fading. This may lead the secondary users to make wrong decision on whether to transmit or not. Numerical results show that conservative interference threshold should be set to control the aggregate interference at the primary victim when fading uncertainty is present.

According to the power density model the precise location and power levels of the secondary transmitters can be neglected. The secondary deployment area and the power density are sufficient to describe the aggregate interference distribution. We noticed that the area where the aggregate interference is computed should contain relatively many secondary transmitters and the channel model should not change. If the number of transmitters is small, the power density approximation may not be accurate. However, for a small number of secondary transmitters the computation by considering the exact locations of the transmitters and their power levels has low complexity.

For decentralized interference control the entire interference margin can be divided among multiple secondary areas or networks. In the present deliverable we derive an equation that relates the power density and the interference margin allocated to an area. In our derivation the aggregate interference from an area is modelled as a log-normal RV. The parameters of the log-normal distribution were derived by using the FW approximation method. It is a matter of further research to derive the relations between the interference margin and the power density also for other distributions of the aggregate interference.

When the terrain morphology is considered, the power density method may not be accurate for describing the aggregate interference from a large secondary area. The reason being, that secondary transmissions far from each other may experience different propagation conditions. However, neighbouring secondary transmitters are attenuated by the same obstacles and have similar path loss values to the TV test points. Because of that, neighbouring transmitters can be grouped together and the power density model is still applicable. The database can control the aggregate interference by controlling the emitted power density from each group of secondary transmitters. The clustering algorithm proposed in the present deliverable is quite simple and it is used to demonstrate the feasibility of the proposed method. It is a matter of future research to test more advanced clustering algorithms for deciding which secondary transmitters can be grouped together.

One of the main objectives of QUASAR is to provide inputs to CEPT. In the present deliverable it is shown that the existing ECC approach for secondary power allocation may violate the TV protection criteria. On the other hand, the power density model has built-in interference control since the power allocation is based on the interference margin available at the primary receivers. In addition, the power density approach can result in higher transmission power levels compared to the ECC method because it can prohibit transmissions in nearby secondary pixels. Our findings have been reported to SE43.

Also, we extended the power density model to incorporate the secondary network's self-interference. Then, we studied the impact of self-interference on power allocation for a secondary cellular system's downlink. We noticed that the power levels become approximately the same for all the cellular base stations. The FCC rule appears to capture the general trend because it allocates a fixed transmission power level outside of the TV protection area. However, the common transmission power level should not be set arbitrarily equal to 4 W, as proposed by FCC, but according to the interference margin available at the borders of the TV and of the secondary cells.

In a realistic environment the distribution of the aggregate interference highly depends on the terrain and the spatial distribution of the service demand. A homogeneous PPP model is not sufficient to capture the non-uniform spatial service demand and the different propagation conditions inside the secondary deployment area. A clustered PPP with relatively few clusters is able to capture the impact of non-uniform user density and to approximate sufficiently well the actual interference distribution. The next step would be to consider the impact of WLAN MAC into the aggregate interference distribution.

7 References

[1] QUASAR deliverable D1.1, "Models, Scenario, Sharing Schemes".

[2] S. C. Schwartz and Y. S. Yeh, "On the distribution function and moments of power sums with log-normal components," Bell System Technical Journal, vol. 61, pp. 1441 – 1462, Sept. 1982.

[3] P. M. Shankar, "Outage probabilities in shadowed fading channels using a compound statistical model," IEE Proceedings Communications, vol. 152, no. 6, pp. 828 – 832, Dec. 2005.

[4] A. Annamalai, C. Tellambura and V.K. Bhargava, "Simple and accurate methods for outage analysis in cellular mobile radio systems – a unifoed approach", IEEE Trans. Commun., vol. 49, no. 2, pp. 303-316, Feb. 2011.

[5] J. Zander, "Performance of optimum transmitter power control in cellular radio systems," IEEE Transactions on Vehicular Technology, vol. 41, no. 1, pp. 57 – 62, Feb. 1992.

[6] A. Ghasemi, "Interference characteristics in power control cognitive radio networks", in Proc. IEEE Crowncom 2010.

[7] A. Ghasemi, "Statistical characterization of interference in cognitive radio networks", in Proc. IEEE PIMRC 2008.

[8] K. Gilhousen, I. Jacobs, R. Padovani, A. Viterbi, J. Weaver, L.A., and I. Wheatley, C.E., "On the capacity of a cellular CDMA system," IEEE Transactions on Vehicular Technology, vol. 40, no. 2, pp. 303 – 312, May 1991.

[9] P. Cardieri, "Modeling interference in wireless ad hoc networks," IEEE Communications Surveys and Tutorials, vol. 12, no. 4, pp. 551 – 572, 2010.

[10] J. G. Andrews, R. K. Ganti, M. Haenggi, N. Jindal, and S. Weber, "A primer on spatial modeling and analysis in wireless networks," IEEE Communications Magazine, vol. 48, no. 11, pp. 156 – 163, Nov. 2010.

[11] F. Baccelli and B. Błaszczyszyn, Stochastic geometry and wireless networks, Volume II — Applications. Foundations and Trends in Networking. NoW Publishers, 2009, vol. 4, No 1–2.

[12] Y.-C. Cheng and T.G. Robertazzi, "A new spatial point process for multihop radio network modeling," Proc. 1990 IEEE International Conf. Comm., pp.1241-1245.

[13] A. Busson and G. Chelius, "Point processes for interference modeling in CSMA/CA ad-hoc networks," In Proceedings of the 6th ACM symposium on Per-formance evaluation of wireless ad hoc, sensor, and ubiquitous networks (PE-WASUN '09). ACM, New York, NY, USA, 33-40. 2009.

[14] D. Stoyan,W. Kendall, and J. Mecke, Stochastic Geometry and Its Applications, 2nd Edition. John Wiley ans Sons Ltd, Chichester, UK, 1996.

[15] N. Shankar and C. Cordeiro, "Analysis of aggregated interference at DTV receivers in TV bands," in International Conference on Cognitive Radio Oriented Wireless Networks and Communications (CrownCom 2008), May 2008, pp. 1 – 6.

[16] N. Hoven and A. Sahai, "Power scaling for cognitive radio," in International Conference on Wireless Networks, Communications and Mobile Computing, vol. 1, June 2005, pp. 250 – 255.

[17] M. Vu, N. Devroye, and V. Tarokh, "On the primary exclusive region of cognitive networks," IEEE Transactions on Wireless Communications, vol. 8, no. 7, pp. 3380 – 3385, July 2009.

[18] X. Hong, C.-X. Wang, and J. Thompson, "Interference modeling of cognitive radio networks," in IEEE Vehicular Technology Conference (VTC 2008-Spring), May 2008, pp. 1851 – 1855.

[19] S. S. Szyszkowicz and H. Yanikomeroglu, "Analysis of interference from large clusters as modeled by the sum of many correlated lognormals," in IEEE Wireless

Communications and Networking Conference (WCNC 2008), April 2008, pp. 741 – 745.

[20] A. Papoulis, Probability, random variables, and stochastic processes, 3rd ed. McGraw-Hill International Editions, 1991.

[21] QUASAR Deliverable D2.4 "Detection performance with multiple secondary interference," public deliverable, 31 March 2012. Available online: http://www.quasarspectrum.eu/downloads/public-deleverables.html

[22] QUASAR Deliverable D4.1 "Sharing strategies for unaware secondary systems," public deliverable, 31 March 2011. Available online: http://www.quasarspectrum.eu/downloads/public-deleverables.html

[23] QUASAR Deliverable D4.2 "Cooperation Strategies for Secondary Users," 31 March 2012. Available online: http://www.quasarspectrum.eu/downloads/public-deleverables.html

[24] P. Pirinen, "Statistical power sum analysis for nonidentically distributed correlated lognormal signals," in The 2003 Finnish signal processing symposium (FINSIG'03), Tampere, Finland, May 19 2003, pp. 254–258.

[25] J. Wu, N. B. Metha, and J. Zhang, "A flexible lognormal sum approximation method," in IEEE Global telecommunications conference (Globecom), St. Louis, MO, USA, November 28 – December 2 2005, pp. 3413 – 3417.

[26] L. Fenton, "The sum of log-normal probability distributions in scatter transmission systems," IRE Trans. Comm. Syst., vol. 8, no. 1, March 1960.

[27] N. C. Beaulieu, A. A. Abu-Dayya, and P. J. McLane, "Estimating the distribution of a sum of independent lognormal variables," IEEE Trans. Communications, vol. 43, no. 12, pp. 2869–2873, December 1995.

[28] G. A. Hufford, A. G. Longley and W. A. Kissick, "A guide to use of the irregular terrain model in the area prediction mode," Technical report 82-100, NTIA, 1982.

[29] P.C. Pinto, M.Z. Win, "Communication in a Poisson Field of Interferers Part II: Channel Capacity and Interference Spectrum," IEEE Trans. on Wireless Commun., vol. 9, no. 7, pp. 2187-2195, Jul. 2010.

[30] A. Ghasemi and E. S. Sousa, "Interference Aggregation in Spectrum-Sensing Cognitive Wireless Networks," IEEE Journal of Selected Topics in Signal Processing, vol. 2, no. 1, Feb. 2008.

[31] A. Rabbachin, T. Q. S. Quek, H. Shin, and M. Z. Win, "Cognitive Network Interference," IEEE Journal on Selected Areas in Communications, vol. 29, no. 2, Feb. 2011.

[32] K. W. Sung, M. Tercero, and J. Zander, "Aggregate Interference in Secondary Access with Interference Protection," IEEE Communications Letters, vol. 15, no. 6, pp. 629–631, Jun. 2011.

[33] J. Kingman, "Poisson Process," Oxford University Press, 1993.

[34] E. Obregon, K. W. Sung, and J. Zander, "On the Feasibility of Low-Power Secondary Access to 960-1215 MHz Aeronautical Spectrum," working paper, 2012.

[35] M. Tercero, K. W. Sung, J. Zander, "Aggregate Interference from Secondary Users with Heterogeneous Density," in proc. IEEE PIMRC, Toronto, Canada, Sep. 2011.

[36] M. Tercero, K. W. Sung, and J. Zander, "Impact of Aggregate Interference on Meteorological Radar from Secondary Users," in proc. IEEE WCNC 2011, Cancun, Mexico, Mar. 2011.

[37] M. Tercero, K. W. Sung, and J. Zander, "Temporal Secondary Access Opportunities for WLAN in Radar Bands," in proc. WPMC 2011, Brest, France, Oct. 2011.

[38] M. Aljuaid and H. Yanikomeroglu, "Impact of Secondary Users Field Size on Spectrum Sharing Opportunities," in proc. IEEE WCNC, Sydney, Austrailia, Apr. 2010.

[39] QUASAR deliverable D5.2, "Methods and tools for estimating spectrum availability: case of single secondary user," Dec. 2011.

[40] K. W. Sung, E. Obregon, and J. Zander, "On the Requirements of Secondary Access to 960-1215 MHz Aeronautical Spectrum," in proc. IEEE DySPAN, Aachen, Germany, May 2011.

[41] M.-J. Ho and G. Stuber, "Co-channel interference of microcellular systems on shadowed Nakagami fading channels," in proc. IEEE VTC, Secaucus, USA, May 1993.

[42] ECC, Report 159 (under public consultation): Technical and operational requirements for the possible operation of cognitive radio systems in the white spaces of the frequency band 470-790 MHz, Sept. 2010.

[43] In the Matter of Unlicensed Operation in the TV Broadcast Bands: Second Memorandum Opinion and Order, Federal Communications Commission, FCC 10-174, Sept 2010, http://hraunfoss.fcc.gov/edocs\ public/attachmatch/FCC-10-174A1.pdf.

[44] Kristen Woyach, Pulkit Grover, and Anant Sahai, "Near vs far field: interference aggregation in TV whitespaces Extended Edition", IEEE Globecom 2011.

[45] RF Signal Propagation, Loss, And Terrain analysis tool for the spectrum between 20 MHz and 20 GHz. Available at http://www.qsl.net/kd2bd/splat.html.

[46] Digital elevation terrain data for North Eurasia, Available at: http://www.viewfinderpanoramas.org/dem3.html#eurasia

[47] K. Ruttik, K. Koufos and R. Jäntti, "Modeling of the secondary system's generated interference and studying of its impact on the secondary system design," J. Radio Eng., Vol. 19, No. 4, Dec. 2010.

[48] R. Jäntti, J. Kerttula, K. Koufos and K. Ruttik, "Aggregate interference with FCC and ECC white space usage rules: case study in Finland", in Proc. IEEE DySPAN 2011.

[49] K. Ruttik, K. Koufos and R. Jäntti, "Computation of aggregate interference from multiple secondary transmitters," IEEE Commun. lett., Vol 15, no. 4, pp. 237-239, Apr. 2011.

[50] S. Saunders, "Antennas and Propagation for Wireless Communication Systems," John Wiley and Son, 2007.

[51] V. Graziano, "Propagation correlations at 900 MHz," IEEE Trans. Veh. Technol., vol. 27, pp. 182-189, Nov. 1999.

[52] T.B. Sorensen, "Slow fading cross-correlation against azimuth separation of base stations," IEE Electronic letters, vol. 35, no. 2, Jan. 1999.

[53] K. Zayana and B. Guisnet, "Measurements and modelisation of shadowing cross-correlations between two base stations," in Proc. Int Conf. Universal Personal Commun., Oct. 1998, pp. 101-105.

[54] K. Gulati, B.L. Evans, J.G. Andrews and K.R. Tinsley "Statistics of Co-Channel Interference in a Field of Poisson and Poisson-Poisson Clustered Interferers," IEEE Trans. on Signal Processing, vol. 58, no. 12, Dec. 2010.

[55] S. Boyd and L. Vandenberghe, Convex Optimization, Cambridge University Press, 2004.

[56] K. Harrison and A. Sahai, "Potential collapse of whitespaces and the prospect for a universal power rule," Proceedings of the Fifth IEEE International Symposium on New Frontiers in Dynamic Spectrum Access Networks, May 2011.